

Oceanic cooling recorded in shells spanning the Medieval Climate Anomaly in the subtropical eastern North Atlantic Ocean

Wesley G. Parker^{a, 1, *}, Yurena Yanes^a, Eduardo Mesa Hernández^b, Donna Surge^c

^a University of Cincinnati, Cincinnati, OH, USA

^b Universidad de La Laguna, San Cristobal de La Laguna, Canary Islands, Spain

^c University of North Carolina, Chapel Hill, NC, USA

ARTICLE INFO

Article history:

Received 25 January 2020

Received in revised form

28 September 2020

Accepted 29 September 2020

Available online xxx

Keywords:

Phorcus atratus

Medieval climate anomaly

Stable isotopes

Paleoclimatology

Holocene

North Atlantic

ABSTRACT

The Medieval Climate Anomaly (MCA; 900–1300 AD) was the most recent period of pre-industrial climatic warming in the northern hemisphere, and thus estimations of MCA signals can illuminate possible impacts of anthropogenic climate change. Current high-resolution MCA climate signals are restricted to mid- and high-latitude regions, which confounds inferences of how the MCA impacted some global/hemispheric climate mechanisms (e.g. North Atlantic Oscillation; NAO). To address this knowledge gap, we estimate seasonally-resolved sea surface temperatures (SSTs) from the oxygen isotope composition ($\delta^{18}\text{O}$) of serially sampled *Phorcus atratus* shells from archaeological sites spanning the MCA in the Canary Islands. Twelve archaeological and six modern *P. atratus* shells were analyzed, and archaeological shells were dated using carbonate-target radiocarbon dating. SSTs were estimated using the published aragonite-water equilibrium fractionation equation. Modern shells showed a mean SST of 20.0 ± 1.5 °C, with a seasonal amplitude of 5.3 ± 0.9 °C. Archaeological shells exhibited a mean SST of 18.2 ± 0.7 °C, with a mean seasonal amplitude of 5.5 ± 1.0 °C. Thus, shells that span the MCA in the Canary Islands recorded SSTs that were significantly cooler than the modern ($P < .05$), contrasting with warming estimates and model predictions elsewhere in the Northern Hemisphere. We propose that the observed cooling resulted from increased upwelling in NW Africa due to a strengthening of the prevailing westerlies and coastal winds along the African shoreline. The intensified upwelling scenario during the MCA is partially supported by in-situ carbon isotope data ($\delta^{13}\text{C}$) retrieved from the archaeological shells, which was compared to the $\delta^{13}\text{C}$ values of modern shells and dissolved inorganic carbon in the ambient seawater. These results are consistent with other low-latitude temperature/precipitation anomalies associated with a positive NAO mode, suggesting a transition to a positive NAO index during the middle and late MCA that possibly extended later into the 13th century AD.

Credit author statement

Wesley G. Parker: Conceptualization, Methodology, Investigation, Data curation, Writing - original draft, Writing - review & editing, Yurena Yanes: Conceptualization, Methodology, Resources, Supervision, Funding acquisition, Writing - review & editing, Eduardo Mesa Hernández: Conceptualization, Writing - review & editing, Donna Surge: Methodology, Funding acquisition, Writing - review & editing.

1. Introduction

Global hydrological and atmospheric circulation patterns fluctuate through time due to the confluence of natural forcing mechanisms like Earth's orbit, volcanic forces, and solar irradiance (Berger, 2013; Crowley, 2000; Friis-Christensen and Lassen, 1991). These climatic variations result in cyclic periods of warming and cooling that can have dramatic impacts on the temperature ranges and precipitation patterns that support terrestrial and marine ecosystems, as well as the human societies that rely upon them (Cullen et al., 2000; Douglas et al., 2015; Harley et al., 2006; Mann et al., 2009). Changes in these patterns can lead to resource scarcity that can eventually drive ecosystem and societal collapse (Bellard et al., 2012; Harley et al., 2006; Mann, 2007; Patz et al., 2005).

* Corresponding author.

E-mail address: wesley.parker@mail.mcgill.ca (W.G. Parker).

¹ Present Address: McGill University, Montréal, QC, Canada.

As Earth enters a phase of anthropogenic global warming, studies of how past climate changes impacted ecosystems and environments are increasingly critical to improve predictions of future climate change, its driving forcing mechanisms, and its long-term impacts on the biosphere (Jones and Mann, 2004). The majority of published paleoclimate data of the recent past is resolved to a single-season, annual scale or coarser resolution, whereas few year-round, seasonally-resolved records have been published, and are particularly scarce in low-latitude regions. High-resolution paleotemperature proxies that track both winter and summer temperatures are especially useful for investigating climatic mechanisms that vary seasonally throughout the year, like the North Atlantic Oscillation (NAO).

The NAO is a major atmospheric forcing mechanism that dictates prevailing wind strength and precipitation distribution across the North Atlantic Basin, including in North America, Europe, and the Middle East/North Africa region (Drinkwater et al., 2003; García Herrera et al., 2001; Hurrell et al., 2003; Kushnir and Wallace, 1989; NOAA, 2018; Trouet et al., 2009). The NAO is defined by the relative difference in atmospheric pressure (at sea-level) between the Azores high-pressure and the Icelandic low-pressure system, which is in turn forced by differential radiative forcing between the tropical (Azores) and polar (Icelandic) latitudes. This meridional pressure gradient is known as the “NAO north-south dipole.” The NAO varies seasonally as changes in temperature drive air pressure differentials. Thus, resolved sea surface temperature (SST) profiles (which are linked to the pressure of overlying airmasses) can contribute to a broader understanding of how NAO dynamics have changed over the past two millennia, and how this may relate to established climatic intervals, such as the Medieval Climate Anomaly (MCA; 900–1300 AD).

Current knowledge of the MCA indicates that this was a period of global climate reorganization, with pronounced warming in the high-latitude North Atlantic (Lamb, 1965; Mann et al., 2009), increased cool-season precipitation in the British Isles (Lamb, 1965), warming and drying in California (LaMarche, 1974), cooling and reduced winter precipitation in Central Asia (Graham et al., 2011; Mann et al., 2009), and cooler SSTs in the central and Eastern Equatorial Pacific (Cobb et al., 2003; Rein et al., 2004). This global-scale climate reorganization has been connected to circulation pattern changes in the Indo-Pacific warm pool, strengthening of the El Niño/Southern Oscillation phenomenon, variation in the NAO, and strengthening of the North Atlantic meridional overturning circulation (Cronin et al., 2010; Graham et al., 2011; Surge and Barrett, 2012; Wanamaker et al., 2012).

Multiproxy approaches for assessing decadal-to centennial-scale variations in temperature during the MCA were compiled by Mann et al. (2009), and were subsequently used to model spatially resolved large-scale relative changes in temperature. This climate model is both compelling and robust but is derived from annually to decadal resolved proxy datasets and lacks sufficient proxy data from the tropical to subtropical North Atlantic region. Accordingly, this model presents limitations regarding the prediction of the NAO mode during the MCA. To rectify these knowledge gaps, this study presents high-resolution SST profiles derived from the Canary Islands—located within the subtropical latitudes of the Northeastern Atlantic Ocean—to illuminate the climate signals of the MCA at the high-pressure endmember of the NAO dipole.

The Canary Islands of Spain are a subtropical archipelago in the Northeast Atlantic near the coast of Morocco. The islands hosted aboriginal populations prior to their annexation by the Spanish, and this aboriginal population generated marine shell-rich deposits (shell middens) across the islands. The temporal origin of Canarian shell middens spans the entire length of aboriginal inhabitation in the archipelago (2500 BP to 700 BP) and includes middens dated to

the MCA (Maca-Meyer et al., 2004; Parker et al., 2018). Additionally, these middens include shells from the edible gastropod *Phorcus atratus* Wood, 1828, which has been shown to reliably track year-round SSTs due to the precipitation of its shell in oxygen isotope equilibrium with ambient seawater (Mesa Hernández, 2008, 2006; Parker et al., 2018, 2017; WoRMS Editorial Board, 2018). Thus, the objective of the present study is to use high-resolution, reconstructed SST profiles derived from the oxygen isotope ratios ($\delta^{18}\text{O}$) from *P. atratus* shells to assess mean annual and seasonal SSTs during the MCA in the Canary Islands, Spain, and compare them to modern SSTs in the region.

This research is driven by the following hypotheses: 1) the seasonal amplitude of SST will be slightly larger during the MCA compared to the modern, following the results of Surge and Barrett (2012) in the high-latitude Orkney archipelago of Scotland; and 2) that mean annual SSTs will be analogous (within analytical error) to modern SSTs, as was predicted by the climate model produced by Mann et al. (2009). Additionally, we present time-series of stable carbon isotope ratios ($\delta^{13}\text{C}$) for each shell to investigate possible changes in upwelling in the study area through time and to screen for possible metabolic isotope effects (Swart, 1983). Our study presents the first high-resolution SST profile for the MCA in the subtropical Northeast Atlantic and contributes to ongoing research regarding NAO dynamics in the North Atlantic by providing SST profiles during the MCA near the Azores high-pressure endmember of the NAO dipole.

2. Background information

2.1. Climatic and oceanographic context

The Canary Islands are a volcanic, oceanic archipelago located near the western coast of Morocco in NW Africa, between 27°37' and 29°25' N and 13°20' and 18°10' W (Fig. 1A). The Canary Islands sit astride the Canary Current, a cold, south-flowing eastern boundary current that originates from the Gulf Stream and propagates southward along the Western European and North African coastlines, bringing cool water and humid air masses to the archipelago (García Herrera et al., 2001). The archipelago is also located immediately adjacent to the NW African coastline, a region of perpetual upwelling that brings cold, nutrient-rich water to the surface (Barton et al., 1998; Villanueva Guimerans and Ruiz Cañavate, 1994). This results in an east-west SST temperature gradient across the archipelago, with the eastern islands experiencing an annual average SST of ~18.5 °C, while the western islands experience SSTs that are ~2 °C warmer (Villanueva Guimerans and Ruiz Cañavate, 1994). The overall climate in the archipelago is classified as a subtropical oceanic climate, with low-moderate rainfall (200–700 mm/yr) and mild air temperatures year-round (15–28 °C) (García Herrera et al., 2001). The Canary Islands are also influenced by the poleward limits of the Hadley cell, the nearby Azores anticyclone (high-pressure system), and the northernmost extension of the Intertropical Convergence Zone (Barton et al., 1998; García Herrera et al., 2001; Marzol, 2008; Navarro-Pérez and Barton, 2001; Sperling et al., 2004).

The focal island in the presented research—Tenerife—is located in the geographic center of the archipelago (28°17' N, 16°37' W) and is the largest island by land area (2030 km²) and elevation (3718 m) (Ancochea et al., 2003; García Herrera et al., 2001). Average annual precipitation is low across the island (~225 mm/yr); however, local precipitation varies dramatically by geospatial location (from 90 to 300 mm/yr) (Bueno and Carta, 2006; Otto et al., 2006; Sperling et al., 2004). Fairly stable precipitation and temperature regimes provided ideal circumstances for the aboriginal settlement of the

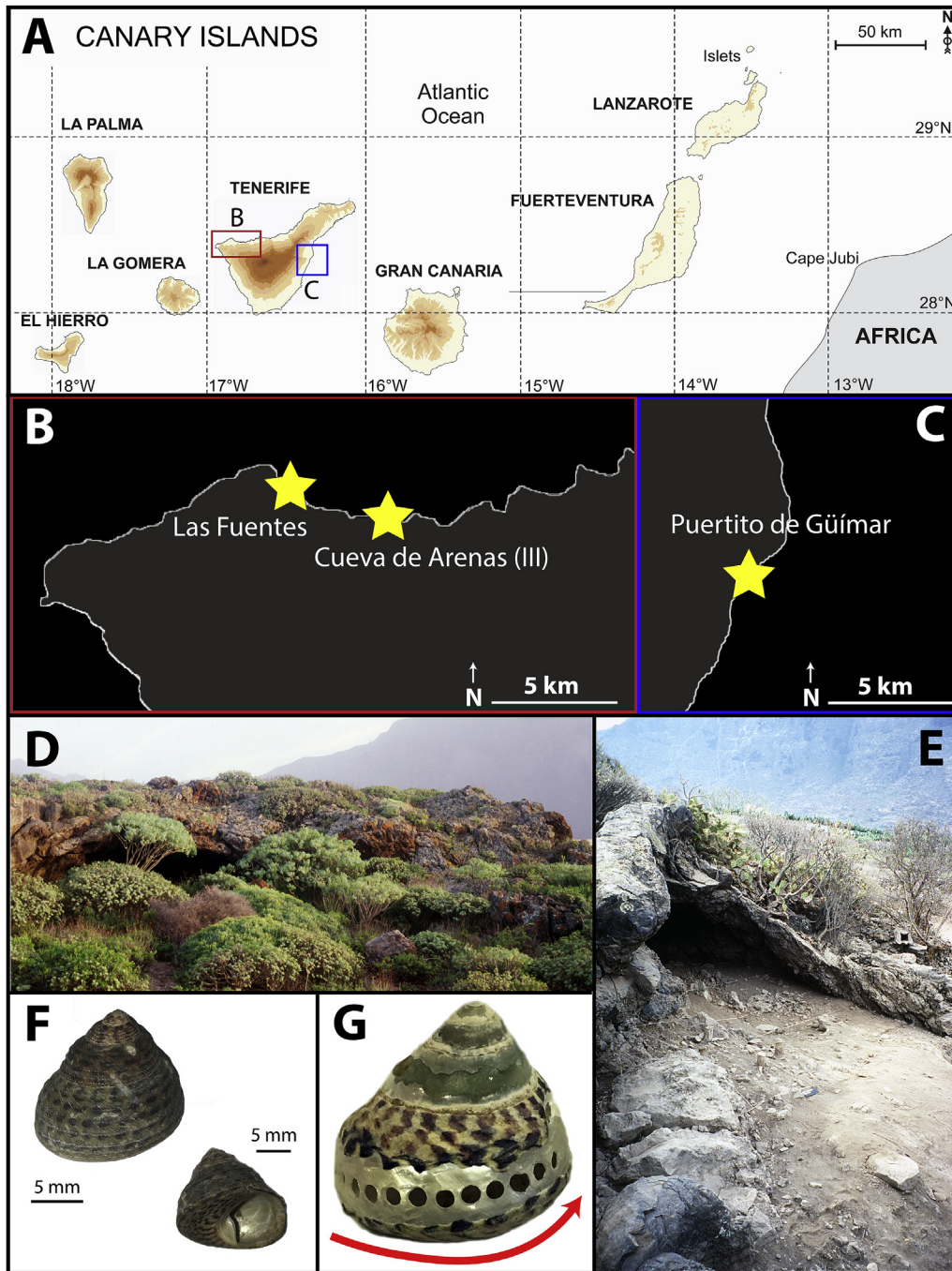


Fig. 1. A) The Canary Islands relative to the coast of NW Africa. Focal regions of Tenerife island are denoted by red and blue boxes. B) The Buenavista del Norte Archaeological Province of NW Tenerife from which all archaeological shells were retrieved for this study. The field sites (Las Fuentes and Cueva Arenas III) are denoted by yellow stars. C) The modern locality of Puertito de Güímar (denoted by a yellow star), on the southeast coast of Tenerife, from which all modern specimens were retrieved in 2012. D) A photograph of the entrance to the Las Fuentes site. E) A photograph of the entrance to the Cueva de Arenas III site. F) Top left: a dorsal view of a modern specimen of *Phorcus atratus* with the apex visible. Bottom right: a basal view of a modern specimen of *P. atratus* with the aperture visible. G) A side view of an archaeological specimen of *P. atratus* with the outer calcite layer removed and aragonite aliquots removed at 1 mm intervals. The red arrow denotes sampling direction from shell margin toward the apex. (For interpretation of the references to colour in this figure legend, the reader is referred to the Web version of this article.)

island that occurred prior to Spanish arrival in the 15th century.

2.2. Archaeological context

The aboriginal population of the archipelago arrived by boat approximately 2500 years BP (defined as years before 1950 AD), and are descended from NW African Berber peoples, although

mtDNA studies have established genetic lineages that can be traced back to Mediterranean Europe, Southwest Asia, and Sub-Saharan Africa (Fregel et al., 2009; Maca-Meyer et al., 2004; Pinto et al., 1996; Rando et al., 1999). The aboriginal population arrived first on the eastern islands before propagating westward across the archipelago (Flores et al., 2001; Mercer, 1980). After initial dispersal, there was little interisland communication, as evidenced

by: 1) a lack of seafaring vessels in the archaeological record; 2) distinctly different cultures, social hierarchy structures, and agricultural practices between islands; and 3) mtDNA analyses that established little genetic mixing between populations on different islands (Arnay-de-la-Rosa et al., 2009; Fregel et al., 2009; Maca-Meyer et al., 2004; Mercer, 1980). The aboriginal communities that lived on Tenerife are known collectively as the “Guanches”, and they had one of the largest, most complex, and hierarchical social systems in the Canary Islands (Arnay-de-la-Rosa et al., 2010, 2009; Maca-Meyer et al., 2004). The island hosted an estimate of 15,000–20,000 inhabitants at its peak population prior to Spanish conquest, and the population was reliant on an agricultural and goat-farming economy, complemented by marine protein sources (Arnay-de-la-Rosa et al., 2010; Aufderheide et al., 1992).

This reliance on marine protein sources, most notably marine gastropods of the genera *Patella* and *Phorcus*, resulted in widely-distributed shell middens, which are large accumulations of shell material that were collected for gastronomic purposes and then discarded after the meat was removed from the shell (Mesa Hernández, 2006). Canary shell middens are populated by multiple taxa of edible gastropods, including *Patella candei* d'Orbigny, 1840 (formerly *Patella crenata*), *Phorcus atratus* (formerly *Osilinus atratus*), and *Stramonita haemastoma* Linnaeus 1767 (formerly *Thais haemastoma*) (Mesa Hernández, 2008, 2006; Parker et al., 2018; WoRMS Editorial Board, 2018). These middens are located along coastal bluffs, sea cliffs, beaches, rock shelters, and caves, and often exhibit high-quality preservation due to shelter from the destructive influences of wave and wind energy (Andrus, 2011; Mesa Hernández, 2008, 2006).

Tenerife's shell middens are particularly useful for studying the MCA because $\delta^{18}\text{O}$ values retrieved from *Phorcus atratus* shells have been shown to be a reliable indicator of paleotemperature (Parker et al., 2017). Moreover, some middens have been radiocarbon dated to confirm that the temporal origin of the shells corresponds to the MCA (Parker et al., 2018). Previously, archaeological research in the archipelago suggested that shell middens were deposited as part of one-time, discrete harvesting events, and would display negligible age-mixing (Mesa Hernández, 2008, 2006; Navarro Mederos et al., 2001). Recently, however, work has shown that some middens may display some degree of age-mixing beyond the boundary of analytical uncertainty, and thus all shell material retrieved for paleoclimate analysis should be individually radiocarbon dated to properly constrain its temporal origins (Parker et al., 2019). Consequently, each shell used in this study has been individually radiocarbon dated to verify MCA origin.

2.3. Ecology of *Phorcus atratus*

Phorcus atratus (Fig. 1F) is a species of prosobranch gastropod that commonly inhabits the rocky intertidal region of the Macaronesian archipelagos (including the Canary Islands). They are slow-moving to stationary browsers that consume algal film (Granado and Caballero, 2001). The shell has an imperforate conical shell with eroded apical whorls and is composed of pearly aragonite (interior) and purple-black calcite (exterior) (Colonese et al., 2009; Prendergast et al., 2013). In the Canary Islands, *P. atratus* are commonly known as “burgados”, or the “topshell” gastropod, due to the likeness of the shell to a spinning top. Fully grown shells of *P. atratus* display 5–6 whorls, with 2 carinae on the ultimate whorl and an oblique aperture. The central columella height ranges between 17 and 23 cm, while the total diameter ranges between 16 and 19 mm (Tryon, 1889). A recent publication confirmed that shells of *P. atratus* from the Canary Islands grow continuously throughout the year and that the oxygen isotope

composition of the interior aragonitic layer is precipitated in isotopic equilibrium with the ambient seawater with a negligible vital effect (Parker et al., 2017). Their finding was evidenced by the presence of both winter and summer seasons in $\delta^{18}\text{O}$ time-series, and by comparing estimated and instrumentally observed SSTs in modern shells. That publication also reports that *P. atratus* has a lifespan between 1 and 2 years. The inner aragonitic layer is preferentially selected for sampling because growth lines are more identifiable in the aragonite layer. See Parker et al. (2017) for additional details regarding the utility of *P. atratus* as a paleoclimate proxy.

The taxonomic nomenclature of *Phorcus atratus*, other species of the genus *Phorcus*, and their geographical distributions in the Canary Islands are the subject of ongoing debate. Recent scientific evidence suggests that *P. atratus* in the Canary Islands may have been historically misidentified, and that Canary shell middens from Tenerife Island may be dominated by *Phorcus sauciatius* Koch, 1845 (Macías, 2017). In the present study, however, we will use the most broadly used taxonomic name *Phorcus atratus* for simplicity.

3. Methods and materials

3.1. Field collection

Phorcus atratus shells were collected from two archaeological sites and one modern site on Tenerife. Archaeological sites are located in the Buenavista del Norte Archaeological Province in the northwest corner of the island (Fig. 1B). This province hosts more than 50 shell middens believed to span the entire temporal range of human occupation on the islands. Two sites were selected due to sample availability and preservation, as well as documented archaeological context: Las Fuentes (Fig. 1D) and Cueva de Arenas III (Fig. 1E). Archaeological shells ($N = 12$) were collected in spatial and stratigraphic order using the following established archaeological excavation techniques. The sites were divided into 1m by 1m quadrats and stratigraphic layers were characterized where applicable, following standard archaeological procedures at the time (Galván et al., 1999). Las Fuentes was divided into two stratigraphic levels, while Arenas III was divided into three stratigraphic levels. New ages generated in the present work indicate material retrieved from contiguous archaeological layers within a site are chronologically equivalent within radiocarbon analytical error. In-situ bulk shell samples were collected from selected quadrats, following the direction of the field archaeologists. Defined stratigraphic layers within each quadrat were excavated independently and placed into different plastic bags properly labeled and transferred to the University of Cincinnati for laboratory preparation and analysis.

Modern specimens ($N = 6$) were collected from the harbor at Puertito de Güímar on the southern coast of Tenerife (Fig. 1C) during February, July, and November 2012. We chose this site because of its abundant shell material. The organisms were alive at the time of the collection, and thus their collection date corresponds to the date of death (see Parker et al. (2017) for additional details). The entire island of Tenerife falls within one isotherm and exhibits an east-west SST gradient of less than 0.5 °C throughout the year (30-year mean COBE SST dataset, Japan Meteorological Agency, 2006). Accordingly, it is reasonable to assume that modern shells from Puertito de Güímar record analogous temperatures to modern shells from the western margin of the island and are therefore reliable indicators of the island-wide SST.

Seawater samples were also collected at 15-day intervals between 2011 and 2012 at Puertito de Güímar. Samples were filtered in the field through a 0.2 μm paper filter and poured into 12 ml glass vials. Vials were sealed after adding a small aliquot of HgCl_2 to

prevent microorganism growth and carbon isotope fractionation of the DIC. Sealed vials were shipped to the University of Cincinnati for refrigerated storage before analysis.

3.2. Preparation of shell material

Archaeological and modern shells were sampled in the same manner. At the University of Cincinnati, all shells were measured along X, Y, and Z directions and then mechanically cleaned using soft bristled brushes to remove detrital contaminants. Shells were then placed into a J.P. Selecta Ultrasonic bath (Model 3000865) to dislodge internal contaminants. They were sonicated for 4 min, cleaned again with soft bristled brushes, rinsed with deionized water, and set to dry for 24 h at 25 °C. The mineralogical composition of the inner (aragonite) and outer (calcite) layers of the shells was confirmed before and after aliquot acquisition through the combination of Raman spectroscopy, scanning electron microscopy, and X-ray diffraction.

Carbonate aliquots for $\delta^{18}\text{O}_{\text{shell}}$ analysis were extracted using the methodology outlined in Parker et al. (2017), derived from Mannino et al. (2007), Colanese et al. (2009), and Prendergast et al. (2013). After cleaning, the outer calcite layer of the shell was removed using a Dremel® 4000 variable speed rotary tool with an abrasive wheel attachment to expose the underlying aragonite for sampling (Fig. 1G). Aragonite aliquots were drilled using the Dremel® 4000 with a 0.5 mm high speed cutter attachment. The shell margin—corresponding to the final growth prior to organism death—was drilled first. Subsequent aliquots were removed at ~1 mm intervals perpendicular to the direction of growth, culminating near the protoconch (Fig. 1G). Previous research on *P. atratus* indicates that 1 mm of growth along shell ontogeny corresponds to a temporal resolution of 2–4 weeks (Parker et al., 2017). Thus, it can be expected that this sampling resolution is sufficient to constrain sub-monthly fluctuations of $\delta^{18}\text{O}_{\text{shell}}$ values.

Each sample was measured at the Light Stable Isotope Mass Spectrometry Lab in the Department of Geological Sciences at the University of Florida (UF) to determine $\delta^{18}\text{O}_{\text{shell}}$ and $\delta^{13}\text{C}_{\text{shell}}$ values. Remaining shell material of each archaeological shell was sent for carbonate-target radiocarbon analysis at the University of California-Irvine (UCI).

3.3. Stable isotope analysis

Samples were analyzed at UF using a Finnigan-MAT 252 Isotope Ratio Mass Spectrometer coupled with a Kiel III automated carbonate preparation device. Approximately 40–50 μg of carbonate powder was digested in 100% H_3PO_4 (Specific Gravity = 1.92) at 70 °C for 10 min and the resultant CO_2 gas was mass analyzed. Results are presented in standard delta notation ($\delta^{18}\text{O}$ and $\delta^{13}\text{C}$) relative to Vienna Pee Dee Belemnite (VPDB). Isotope standards NBS 19 ($\delta^{18}\text{O} = -2.20\text{‰}$ VPDB; $\delta^{13}\text{C} = 1.95\text{‰}$ VPDB) and NBS 18 ($\delta^{18}\text{O} = -23.01\text{‰}$ VPDB; $\delta^{13}\text{C} = -5.01\text{‰}$ VPDB) were measured repeatedly to calibrate and calculate analytical and experimental precision. Analytical precision was better than $\pm 0.1\text{‰}$, based on repeated measurements of samples and standards throughout the runs.

Seawater samples were analyzed at the University of Kentucky for $\delta^{18}\text{O}$ and $\delta^{13}\text{C}_{\text{DIC}}$ values using a Picarro device and a GasBench II peripheral device interfaced with a Thermo Scientific DeltaV Isotope Ratio Mass Spectrometer, respectively. The $\delta^{18}\text{O}_{\text{seawater}}$ values presented in this research are published, along with the $\delta^{18}\text{O}_{\text{seawater}}$ analysis procedures, in Parker et al. (2017). The analytical uncertainty for $\delta^{18}\text{O}_{\text{seawater}}$ analyses was $\pm 0.1\text{‰}$, and values are reported in per mil units relative to the VSMOW standard.

The seawater $\delta^{13}\text{C}_{\text{DIC}}$ analyses presented in this research were conducted following standard procedures. Accordingly, 3–4 ml aliquots of seawater were transferred to 12 ml septum-capped exetainer vials with a He atmosphere. A few drops of 100% H_3PO_4 (phosphoric acid) were then added to convert DIC into gaseous CO_2 . The generated CO_2 in the headspace was mass analyzed using a continuous flow helium carrier stream in the IRMS via a GasBench II peripheral device. Analytical precision was better than $\pm 0.2\text{‰}$ based on repeated measurements of samples, in-house DIC reference standards, and reference gasses throughout the runs. Values are reported in per mil units relative to the VPDB standard.

3.4. Calculating sea surface temperature

Sea surface temperatures derived from $\delta^{18}\text{O}_{\text{shell}}$ values were calculated using the aragonite-water equilibrium equation:

$$T(^{\circ}\text{C}) = 20.6 - 4.34 (\delta^{18}\text{O}_{\text{arag}} - \delta^{18}\text{O}_{\text{seawater}}) \quad (1)$$

Where $\delta^{18}\text{O}_{\text{arag}}$ is the $\delta^{18}\text{O}$ value of aragonitic shell relative to the VPDB standard and $\delta^{18}\text{O}_{\text{seawater}}$ is the $\delta^{18}\text{O}$ value of the seawater relative to VSMOW minus a correction factor to accommodate the difference between the VPDB and VSMOW scales (Grossman and Ku, 1986). The VPDB-VSMOW correction factor utilized in this report is 0.27‰, as defined by Gonfiantini et al. (1995). We used a constant $\delta^{18}\text{O}_{\text{seawater}}$ value of 0.8‰ (VSMOW), as was previously reported in Parker et al. (2017) because it does not vary significantly through seasons in the Canary Islands. Moreover, published research suggests that $\delta^{18}\text{O}_{\text{seawater}}$ values may vary from 0.8‰ by up to $\pm 0.2\text{‰}$ through the first several hundred meters of the water column (Wilke et al., 2009). Additional discussion of variability in $\delta^{18}\text{O}_{\text{seawater}}$ values are presented in Section 5.1 of this paper. Analytical precision of $\sim 0.1\text{‰}$ results in possible error of ± 0.4 °C based on the slope of Equation (1).

3.5. Radiocarbon analysis

All archaeological shells were radiocarbon dated using the rapid and more affordable carbonate-target methodology at the W.M. Keck AMS laboratory at the University of California, Irvine, following published procedures outlined online at (dos Santos et al., 2018) and in Bush et al. (2013). In this procedure, 0.3 mg of powdered shell material from each aliquot is mixed with 5 mg unbaked pure Nb (Alfa Aesar #40510, -325 mesh, 99.99%). This mixture is poured directly into the aluminum cathode target and pressed for AMS measurement (Bush et al., 2013). Samples processed in this laboratory using traditional graphite-target methodology have exhibited 0.3% precision and 55,000 yr backgrounds, while AMS dates retrieved via paired carbonate-target and graphite-target methods are statistically indistinguishable from the conventional method ($P > .05$) for samples under 10,000 years old (Bush et al., 2013; Culleton et al., 2006; dos Santos et al., 2018; Kowalewski et al., 2017; New et al., 2019). AMS data are reported in ^{14}C age (years BP), and the data were corrected for ^{13}C fractionation per the conventions of Stuiver and Polach (1977).

Radiocarbon dates were calibrated with CALIB 7.1 (Stuiver et al., 2020), using the MARINE13 calibration curve. Shells of *P. atratus* precipitate their shells from multiple carbon sources, most significantly carbon available in the seawater, and thus apparent radiocarbon ages must be corrected for the marine reservoir effect (Poulain et al., 2010; Stuiver et al., 1986; Stuiver and Polach, 1977). The local deviation from the time dependent model calibration curve (ΔR) was determined to be 135 ± 103 yrs, using data from the Marine Reservoir Correction Database (Stuiver et al., 2020). The ΔR was calculated using the geographic proximity to studies of

reservoir effects by Ndeye (2008) and Monges Soares (1993) in nearby Senegal and Iberia, respectively. Calibrated ages are reported using the 2-sigma (2σ ; 95.4% probability) age range.

3.6. Data analysis

SST time-series were calculated for each shell by plotting estimated SST data against distance from shell margin, which serves as a proxy for time. Only the final year of growth for each shell was used for statistical and comparative purposes, and thus maximum, minimum, and mean estimated SSTs are representative only of the final full year of the organism's life. The last year of shell growth was prioritized because all analyzed shells showed lifespans greater than one year, but most were shorter than two years. Thus, most shell time-series include some partial-year data. We elected to exclude the partial years to facilitate direct comparisons between shells, focusing on the last one-year records that are present in all analyzed specimens. The final growth year was highlighted by visually defining one full sinusoidal profile in the SST time-series, thus ensuring that a full annual cycle was included. For shells with unclear sinusoidal trends (TAR(III)-9, T-Modern-2, T-Modern-3), one year of growth was estimated using the average distance (in mm) along ontogeny from shells with visible sinusoidal profiles. Carbon isotope time-series were also generated for each shell. As $\delta^{13}\text{C}_{\text{shell}}$ values do not typically vary seasonally, the same demarcation of a year is applied to both SST and $\delta^{13}\text{C}$ time-series derived from the same shell.

Aggregated comparisons of estimated seawater temperature recorded in modern and archaeological shells and $\delta^{13}\text{C}$ data are presented in the discussion using violin plots. Violin plots combine a box plot and a density trace/smoothed histogram to display the range and structure of data (Hintze and Nelson, 1998). They display the center (median), spread (range), asymmetry (interquartile range), and outliers in both the carbon and oxygen dataset, while simultaneously overlaying a density trace/smoothed histogram to permit interpretation of data distribution (e.g. uniform, bimodal, normal). The presented violin plots were generated using the *vioplot* package in RStudio (Adler and Kelly, 2018; R Core Team, 2017).

The white dot in the center of each violin plot is the median value for each site, while the black rectangle surrounding the white dot represents the interquartile range (IQR) of the data. The vertical length of the black line inside the plot represents the extent of the upper and lower adjacent values ($Q1 - 1.5 \times \text{IQR}$ or $Q3 + 1.5 \times \text{IQR}$), while the total vertical length of the violin represents the total range of data (inclusive of outliers). The contours of the violins represent the relative distribution of the data, with larger horizontal length representative of higher data density (Adler and Kelly, 2018; Hintze and Nelson, 1998).

Table 1
Carbonate-target radiocarbon results.

Shell ID	Locality	Level	Radiocarbon Age		2σ Median Probability Range (Cal. Yrs. AD)	Median Probability Age (Cal. Yrs. AD)
			Yrs. BP	\pm		
TLF-1A	Las Fuentes	L1	1205	40	1090–1470	1310
TLF-1B	Las Fuentes	L1	1160	40	1140–1520	1350
TLF-9A	Las Fuentes	L1	1340	60	970–1410	1190
TLF-9B	Las Fuentes	L1	1210	40	1080–1470	1300
TLF-9C	Las Fuentes	L1	1390	50	900–1340	1140
TLF-16	Las Fuentes	L2	1435	45	870–1310	1100
TLF-23	Las Fuentes	L2	1420	25	900–1310	1120
TAR(III)-9	Cueva de Arenas (III)	L2	1805	15	970–1430	1220
TAR(III)-25	Cueva de Arenas (III)	L2	1340	15	1000–1390	1190
TAR(III)-27	Cueva de Arenas (III)	L2	1275	45	1040–1430	1240
TAR(III)-30	Cueva de Arenas (III)	L2	1275	45	1040–1430	1240
TAR(III)-33	Cueva de Arenas (III)	L2	1455	45	840–1300	1090

Modern and ancient shell SST and $\delta^{13}\text{C}$ data were not normality distributed (Shapiro-wilk test, $P > .05$). Thus, the non-parametric Wilcoxon rank-sum test was employed to assess the difference between modern and ancient SST and $\delta^{13}\text{C}$ data.

4. Results

4.1. Radiocarbon ages

Radiocarbon ages are presented in Table 1. The oldest shell (specimen TAR(III)-33) has a 2σ probability range of 840–1300 cal yrs AD and was retrieved from Level 2 of Arenas III. The youngest shell (specimen TLF-9B) has a 2σ probability range of 1140–1520 cal yrs AD and was retrieved from Level 1 of Las Fuentes. The average upper (lower) boundary of the 2σ probability age range for shells from Las Fuentes is 1400 (990) cal yrs AD and for Cueva de Arenas III is 1400 (980) cal yrs AD. All shells analyzed in this study exhibit 2σ probability ranges that significantly overlap with the MCA (i.e., between 900 and 1300 AD); however, only one shell—TAR(III)-33—has an upper age boundary that does not exceed the upper limit of the MCA. Thus, this paper assumes that all shells are representative of the MCA, but more conservative age constraints reveal that 11 of the 12 shells could have grown 0–220 years after the MCA. Tighter age control is not possible using these shells because of the high (135 ± 103) ΔR value used in the ^{14}C calibration, resulting in large 2σ probability age ranges for all shells.

4.2. Stable isotope time-series of modern shells and seawater

Oxygen and stable carbon isotope ratios for the modern shells and estimated SSTs from the last year of shell growth (one full seasonal cycle) are summarized in Table 2. Raw data are presented in supplementary table S1. The $\delta^{18}\text{O}$ values retrieved from one of the modern shells (specimen Pho-1) were previously published in Parker et al. (2017). This study presents new $\delta^{13}\text{C}_{\text{shell}}$ data from Pho-1 along with $\delta^{18}\text{O}$ and $\delta^{13}\text{C}$ time-series extracted from five new shells. Modern shell-derived SST estimations are plotted in Fig. 2, while observed $\delta^{13}\text{C}_{\text{shell}}$ values are plotted in Fig. 3.

The maximum and minimum $\delta^{18}\text{O}_{\text{shell}}$ values from modern shells are 1.7‰ (Pho-1) and -0.2 ‰ (T-Modern-3), respectively. The calculated minimum and maximum temperature ranges from 15.5 to 23.8 °C. The mean $\delta^{18}\text{O}_{\text{shell}}$ value from milled samples ($N = 172$) is 0.7 ± 0.3 ‰, which corresponds to an estimated SST of 20.0 ± 1.5 °C. The mean seasonality range (i.e., the difference between the coldest and warmest temperature within a full year of growth) is 5.3 ± 0.9 °C. The largest seasonal amplitude (6.5 °C) is observed in specimen T-Modern-1, while the smallest seasonal amplitude (4.6 °C) is observed in T-Modern-5. Four of the modern

Table 2

Summary (minimum, maximum, mean, and standard deviation) of $\delta^{18}\text{O}$, Temperature ($^{\circ}\text{C}$), and $\delta^{13}\text{C}$ from the final year of growth for each modern *Phorcus atratus* shell. SST calculation error = $\pm 0.4^{\circ}\text{C}$, $\delta^{18}\text{O}_{\text{shell}}$ and $\delta^{13}\text{C}_{\text{shell}}$ analytical error = $\pm 0.1\text{‰}$.

Sample ID	# of milled samples included in final year	$\delta^{18}\text{O}$ (‰ VPDB)			Temperature ($^{\circ}\text{C}$)				$\delta^{13}\text{C}$ (‰ VPDB)		
		Max.	Min.	Mean	Max.	Min.	Mean	Range	Max.	Min.	Mean
T-Modern-1	26	1.6	0.1	0.9	22.5	16.0	19.0	6.5	1.4	-1.3	0.0
T-Modern-2	28	1.0	0.1	0.5	22.7	18.4	20.6	4.2	1.5	0.2	1.0
T-Modern-3	28	0.9	-0.2	0.1	23.8	18.9	22.3	4.9	1.6	-0.6	0.7
T-Modern-4	28	1.4	-0.1	0.7	23.2	16.9	20.0	6.3	1.0	-2.7	-0.7
T-Modern-5	28	1.1	0.0	0.6	22.8	18.1	20.3	4.6	0.4	-1.8	-0.7
Pho-1	34	1.7	0.5	1.2	20.5	15.5	17.9	5.0	1.1	-1.8	0.4
Modern Means		1.3	0.1	0.7	22.6	17.3	20.0	5.3	1.2	-1.3	0.1
Standard Deviations (\pm)		0.3	0.2	0.3	1.1	1.4	1.5	0.9	0.5	1.0	0.7

* Shell *Pho-1* was previously reported in [Parker et al. \(2017\)](#).

shells exhibit clearly visible quasi-sinusoidal profiles along the shell's growth axis. In contrast, two modern shells (specimens T-Modern-2 and T-Modern-3) display flatter $\delta^{18}\text{O}$ time-series with more reduced seasonal variability ([Fig. 2](#)). The variability among $\delta^{18}\text{O}_{\text{shell}}$ profiles retrieved from shells of the same age is the focus of ongoing research. Possible explanations for these apparent inconsistencies among shells include organism-specific physiological effects (e.g. deformities within individual shells) or small-scale differences in the organism's environment during growth (e.g.

unusually cold or warm water). To minimize the effect of this discrepancy and obtain a representative average environmental signal we chose to analyze at least five (5) shells per archaeological site. The observed agreement between calculated SSTs from modern shells and instrumentally recorded SSTs reinforces that this approach appears appropriate. Hence, we argue that the calculated SSTs from groups of shells of the same age-group should be representative of the environment in which they grew.

The $\delta^{13}\text{C}_{\text{shell}}$ data from most of the modern shells does not

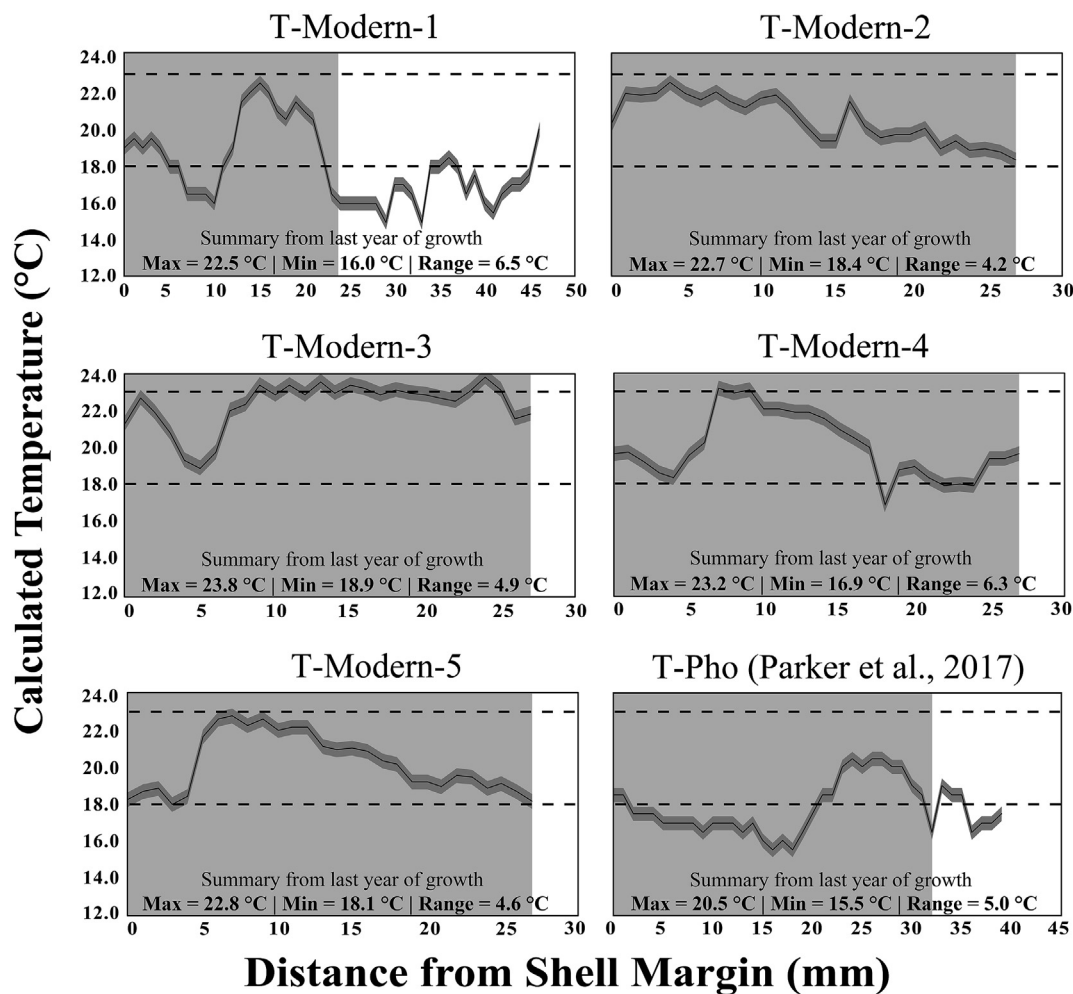


Fig. 2. Calculated SST from live-collected shells retrieved from the rocky intertidal coast in the Canary Islands during 2012. The light gray box depicts the last year of growth, including summer and winter SSTs. Horizontal dashed lines indicate the range of instrumentally measured modern SSTs (18–23 $^{\circ}\text{C}$) from [Parker et al. \(2017\)](#). The dark gray error envelope around the data corresponds to the range of analytical error ($\pm 0.4^{\circ}\text{C}$).

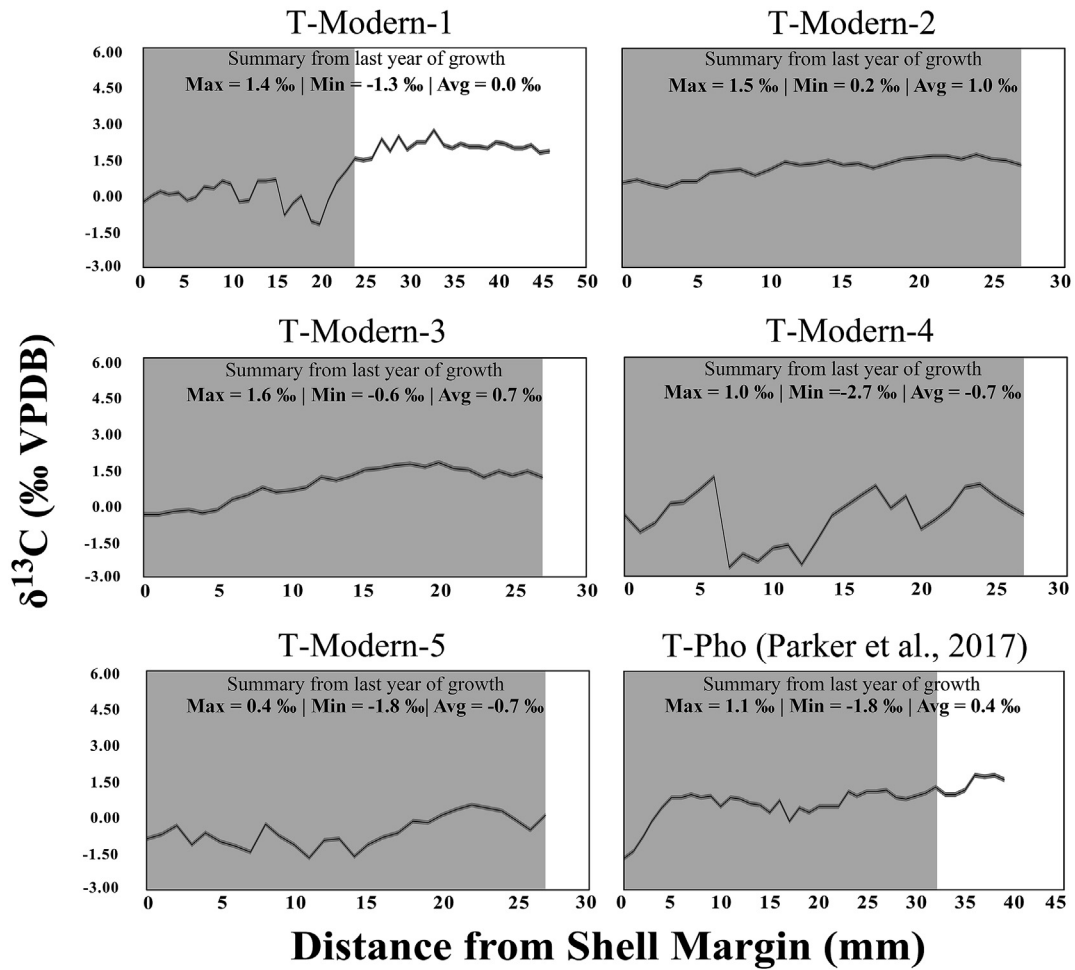


Fig. 3. Observed $\delta^{13}\text{C}$ values from live-collected shells retrieved from the rocky intertidal coast in the Canary Islands during 2012. The light gray box depicts the last year of growth, as defined by summer and winter SSTs (Fig. 2). The dark gray error envelope around the data corresponds to the range of analytical error ($\pm 0.1\%$).

Table 3

Seawater $\delta^{13}\text{C}_{\text{DIC}}$ data from Puertito de Güímar. All $\delta^{13}\text{C}_{\text{DIC}}$ values are presented in ‰ relative to VPDB.

Date of collection	$\delta^{13}\text{C}_{\text{DIC}}$ (‰ VPDB)
16-Jul-11	1.0
1-Aug-11	1.2
15-Aug-11	0.8
31-Aug-11	0.7
15-Sep-11	0.9
29-Sep-11	0.7
16-Oct-11	0.7
1-Nov-11	0.9
16-Nov-11	0.8
2-Dec-11	1.0
17-Dec-11	0.9
1-Jan-12	1.0
14-Jan-12	1.0
31-Jan-12	0.8
16-Feb-12	0.7
3-Mar-12	1.1
15-Mar-12	0.8
Mean	0.9
SD	0.2

exhibit a seasonal variation along the shell's growth axis (Fig. 3). Specimen T-modern-4 shows greater deviation around the median value than the other shell records. The maximum and minimum $\delta^{13}\text{C}_{\text{shell}}$ values are 1.6‰ (specimen T-Modern-3) and -2.7‰

(specimen T-Modern-4), respectively. The mean $\delta^{13}\text{C}_{\text{shell}}$ value from all modern shells combined is $0.1 \pm 0.7\%$.

The $\delta^{13}\text{C}_{\text{DIC}}$ values from seawater are summarized in Table 3. The mean $\delta^{13}\text{C}_{\text{DIC}}$ value in the southeast coast of Tenerife is $0.9 \pm 0.2\%$, ranging from 0.7‰ to 1.2‰. Values show little variability around their means, and do not exhibit any clear seasonal signals. $\delta^{18}\text{O}_{\text{water}}$ values were previously reported in Parker et al. (2017). The mean annual $\delta^{18}\text{O}_{\text{water}}$ value was $0.8 \pm 0.1\%$, and the $\delta^{18}\text{O}_{\text{water}}$ time-series display little variability around the mean value and do not vary seasonally.

4.3. Stable isotope time-series of archaeological shells

Oxygen and carbon stable isotope ratios for the archaeological shells and estimated SSTs of the last year of growth (one full seasonal cycle) are summarized in Table 4. Raw isotopic data and SST estimates are reported in supplementary tables S2 and S3. Calculated SSTs are graphically represented in Fig. 4. The maximum and minimum $\delta^{18}\text{O}$ values are 2.3‰ (specimen TLF-23) and 0.2‰ (specimen TLF-16), respectively. The calculated maximum and minimum temperature ranges from 13.1 °C to 21.9 °C. The mean $\delta^{18}\text{O}$ value for final-growth-year milled samples from archaeological shells (N = 309) is $1.1 \pm 0.2\%$ and corresponds to a temperature of 18.2 ± 0.7 °C. Most shells exhibit a quasi-sinusoidal trend of $\delta^{18}\text{O}_{\text{shell}}$ values. Calculated temperatures along shell main growth

Table 4

Summary (minimum, maximum, mean, and standard deviation) of $\delta^{18}\text{O}_{\text{shell}}$ values, temperature ($^{\circ}\text{C}$), and $\delta^{13}\text{C}_{\text{shell}}$ values from the final year of growth for each archaeological *Phorcus atratus* shell. SST calculation error = $\pm 0.4^{\circ}\text{C}$, $\delta^{18}\text{O}_{\text{shell}}$ and $\delta^{13}\text{C}_{\text{shell}}$ analytical error = $\pm 0.1\text{‰}$.

Sample ID	Level	# of milled samples included in final year	$\delta^{18}\text{O}$ (‰ VPDB)			Temperature ($^{\circ}\text{C}$)				$\delta^{13}\text{C}$ (‰ VPDB)		
			Max.	Min.	Mean	Max.	Min.	Mean	Range	Max.	Min.	Mean
TLF-1A	L1	22	1.5	0.5	1.0	20.7	16.3	18.3	4.4	3.8	2.8	3.3
TLF-1B	L1	25	1.7	0.5	1.2	20.5	15.5	17.7	5.0	3.1	1.5	2.3
TLF-9A	L1	20	1.7	0.3	1.0	21.5	15.4	18.4	6.1	1.5	-1.4	0.7
TLF-9B	L1	35	1.6	0.3	1.0	21.5	15.8	18.6	5.7	4.8	2.2	3.4
TLF-9C	L1	23	1.6	0.5	1.0	20.8	15.9	18.4	4.9	3.5	1.2	3.0
TLF-16	L2	24	1.7	0.2	0.7	21.9	15.6	19.8	6.4	3.3	1.3	2.2
TLF-23	L2	22	2.2	0.9	1.4	19.0	13.1	16.9	5.9	4.1	1.6	3.2
TAR(III)-9	L2	23	1.5	0.7	1.1	20.0	16.6	18.0	3.4	3.3	-2.3	2.2
TAR(III)-25	L2	27	2.0	0.3	1.2	21.8	14.4	17.4	7.4	4.2	2.2	3.2
TAR(III)-27	L2	34	1.8	0.3	1.1	21.7	15.2	18.1	6.4	4.1	2.3	3.5
TAR(III)-30	L2	30	1.7	0.5	1.2	20.6	15.5	17.7	5.1	3.4	1.2	2.2
TAR(III)-33	L2	25	1.7	0.3	1.0	21.4	15.6	18.6	5.8	3.6	1.1	2.5
MCA Means			1.7	0.4	1.1	21.0	15.4	18.2	5.5	3.6	1.1	2.6
Standard Deviations (\pm)			0.2	0.2	0.2	0.8	0.9	0.7	1.0	0.8	1.5	0.8

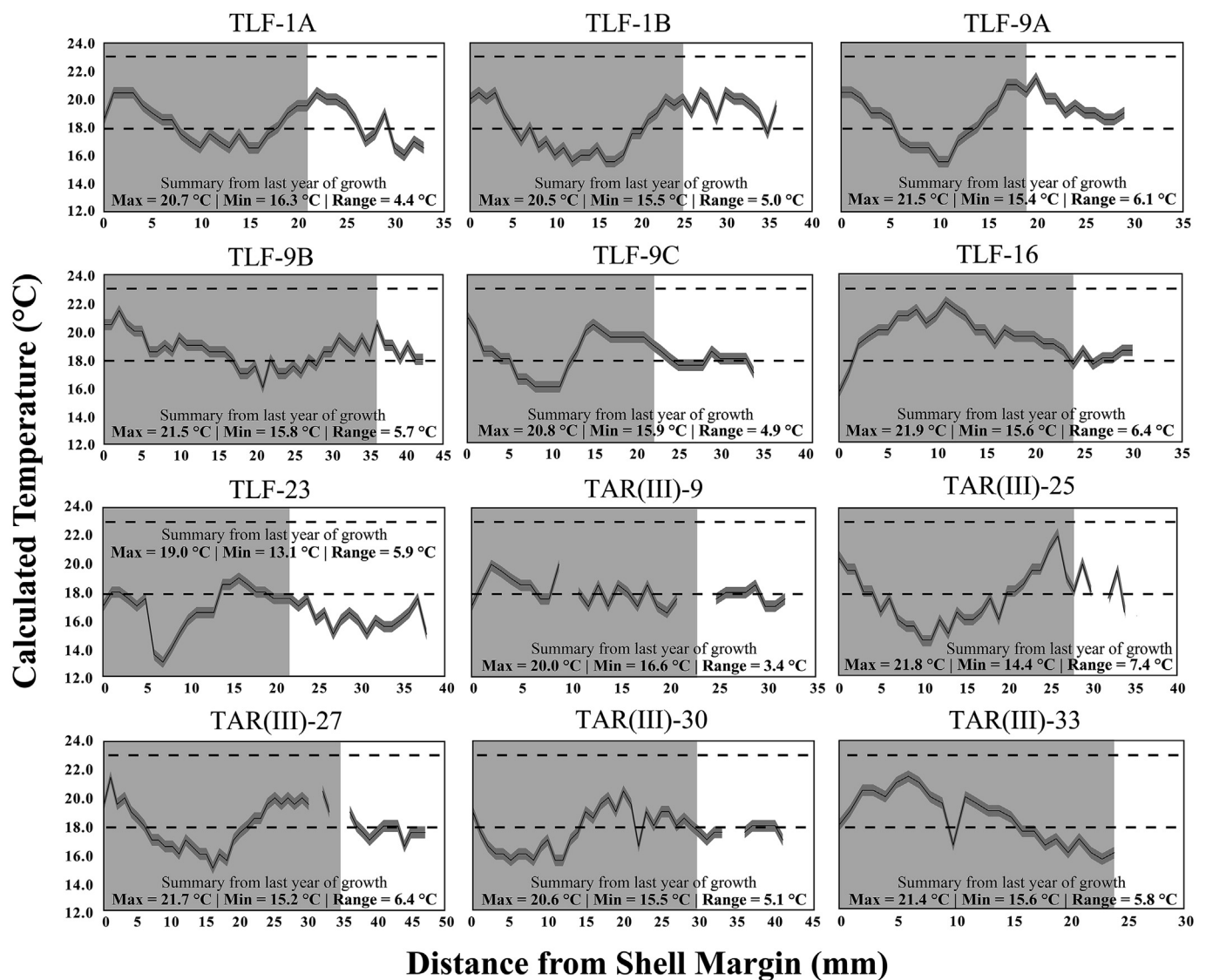


Fig. 4. Calculated SST from shells retrieved from archaeological sites spanning the MCA in the Canary Islands. The light gray box depicts the last year of growth, including summer and winter SSTs. Horizontal dashed lines indicate the range of instrumentally measured modern SSTs (18–23 $^{\circ}\text{C}$) from Parker et al. (2017). The dark gray error envelope around the data corresponds to the range of analytical error ($\pm 0.4^{\circ}\text{C}$).

Estimated Final-Growth-Year Temperatures by Site

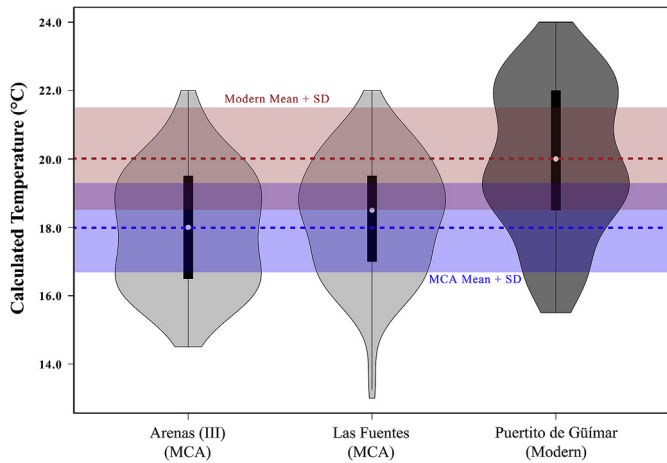


Fig. 5. Violin plot of all estimated temperatures from the final year of growth for all shells in this study. The modern mean (20.0 °C) and archaeological mean (18.2 °C) are denoted by a red and blue dashed line and bar, respectively. The width of the bar corresponds to the standard deviation of each mean (modern SD = 1.5 °C; archaeological SD = 0.7 °C). (For interpretation of the references to colour in this figure legend, the reader is referred to the Web version of this article.)

axis clearly depict winter and summer seasons with specimen TAR(III)-9 showing the least seasonal variability. The mean seasonal amplitude for all archaeological shells combined is 5.5 ± 1.0 °C. The smallest and largest seasonal amplitudes are recorded in specimen TAR(III)-9 (3.1 °C) and TAR(III)-25 (7.4 °C), respectively. The mean SST recorded in archaeological shells is 1.8 °C cooler than the modern mean (Fig. 5). While this 1.8 °C offset is statistically significant (Wilcoxon rank-sum test; $P < .05$), the seasonal amplitude between ancient and modern shells is approximately the same.

As with the modern shells, $\delta^{13}\text{C}_{\text{shell}}$ time-series are relatively flat and do not show a seasonal trend (Fig. 6). The maximum and minimum $\delta^{13}\text{C}$ values are 4.8‰ (specimen TLF-9B) and -2.3‰ (specimen TAR(III)-9), respectively. The mean $\delta^{13}\text{C}$ value for all archaeological shells is 2.6 ± 0.8 ‰, which is ~2.5‰ higher than the mean value of the modern shells (Fig. 7). This 2.5‰ offset between modern and ancient shells is statistically significant (Wilcoxon rank-sum test; $P < .05$).

5. Discussion

5.1. Influences on the isotope geochemistry of shells

The results indicate that both $\delta^{18}\text{O}$ and $\delta^{13}\text{C}$ values differ significantly between modern and archaeological shells, with modern shells reflecting reduced $\delta^{18}\text{O}$ and $\delta^{13}\text{C}$ values relative to the archaeological shells. The $\delta^{18}\text{O}$ and $\delta^{13}\text{C}$ variability in marine shells are impacted by an array of environmental parameters. However, while the environmental controls on $\delta^{18}\text{O}_{\text{shell}}$ values are fairly well studied in the published literature, the controls on shell $\delta^{13}\text{C}$ values are comparatively less understood. In the following paragraphs, we discuss possible environmental influences on shell $\delta^{18}\text{O}$ and $\delta^{13}\text{C}$ values of *P. atratus* in the Canary Islands and identify the likely causes of the observed isotopic offsets between modern and archaeological shells.

The primary factors influencing shell $\delta^{18}\text{O}$ values of marine gastropods include (1) kinetic isotope effect; (2) the calcium carbonate polymorphs present in the shell; (3) the degree of diagenetic alteration; (4) ambient seawater $\delta^{18}\text{O}$ value; and (5) the ambient seawater temperature. Kinetic isotope effects can affect

both the oxygen and carbon isotope ratios due to the preferential uptake of lighter isotopes. In this scenario, carbon isotopes would be expected to covary with oxygen (McConnaughey, 1989a). Because the carbon and oxygen isotope ratios of our shells do not covary, the effects of kinetic isotope effects are considered negligible in this study.

The shells of *P. atratus* are bimineralic, and therefore precipitate their shells using two calcium carbonate polymorphs, an outer calcite layer and an inner aragonite layer (Parker et al., 2017). Different polymorphs of calcium carbonate exhibit distinctive water-carbonate fractionation factors, and thus different paleothermometry equations are proposed (e.g. the water-aragonite equation by Grossman and Ku, 1986, or the water-calcite equation by Friedman and O'Neil, 1977). In the shells of *P. atratus*, the outer calcite layer was carefully removed and only the inner aragonite layer was sampled. Accordingly, the influence of calcite on the $\delta^{18}\text{O}$ values should be insignificant. The sampled material was confirmed to be aragonite through the use of x-ray diffraction and Raman spectroscopy. Additionally, no secondary crystal overgrowth was detected via scanning electron microscopy. Consequently, recrystallization or secondary overgrowth are also unlikely to have influenced the $\delta^{18}\text{O}_{\text{shell}}$ values.

Variations in $\delta^{18}\text{O}$ values of the ambient seawater influences shell $\delta^{18}\text{O}$ values and could explain the isotopic offset between the MCA and modern $\delta^{18}\text{O}_{\text{shell}}$ values. Changes in $\delta^{18}\text{O}_{\text{seawater}}$ values may occur due to: 1) changes in the global ocean $\delta^{18}\text{O}$ values; 2) seasonal variability of local $\delta^{18}\text{O}_{\text{seawater}}$ values as a result of evaporation and precipitation; and 3) the vertical movement of water masses through the water column (e.g. during upwelling or downwelling). The average global ocean $\delta^{18}\text{O}$ value is not expected to have been significantly different between the MCA and today. Previous research indicates that large variations in global $\delta^{18}\text{O}_{\text{seawater}}$ values are generally influenced by changes in ice volume and occur over centennial to millennial timescales that greatly eclipse the temporal scope of the MCA (Thornalley et al., 2009). While some research has found that more rapid variations in seawater $\delta^{18}\text{O}$ values have occurred due to catastrophic, largescale events such as the 8.2kyr event (e.g. Estrella-Martínez et al., 2019a), the MCA has not been shown to be one of these events. Accordingly, as there has been no significant global glaciation between the MCA and the present, it is assumed that the modern global seawater $\delta^{18}\text{O}$ values are analogous to those of the MCA.

Local and seasonal changes in $\delta^{18}\text{O}_{\text{seawater}}$ values are also not expected to have shifted significantly between MCA and today. Evaporation and precipitation show small variations throughout the year in the coastal regions of the Canary Islands (Agencia Estatal de Meteorología, 2020). Parker et al. (2017) found that, while modern seawater $\delta^{18}\text{O}$ values in the Canary Islands ranged from 0.6 to 1.0‰ over the course of a year, $\delta^{18}\text{O}_{\text{seawater}}$ values did not show a distinctive seasonal trend. They reported an average value of 0.8 ± 0.1 ‰ which was representative of the year-round $\delta^{18}\text{O}_{\text{seawater}}$ values in the modern Canary Islands. Accordingly, 0.8‰ was the $\delta^{18}\text{O}_{\text{seawater}}$ value used in the aragonite-water fractionation equation in this study. Furthermore, oxygen isotope records from land snail shells indicates that the hydroclimate of the Canary Islands was largely stable over the past 5000 years (Yanes et al., 2011). Thus, we assume minor variations in evaporation and precipitation throughout the year during the MCA, comparable to the modern coastal sites in the modern Canary Islands.

Vertical movement of water masses with differing $\delta^{18}\text{O}$ values could occur as a result of upwelling and downwelling. Wilke et al. (2009) measured $\delta^{18}\text{O}_{\text{shell}}$ values of modern foraminifera through the water column in the Canary Islands basin between 0 and 500m water depth. They reported $\delta^{18}\text{O}_{\text{seawater}}$ values between 1.0‰ (surface waters) and 0.6‰ (500m water depth), with an average

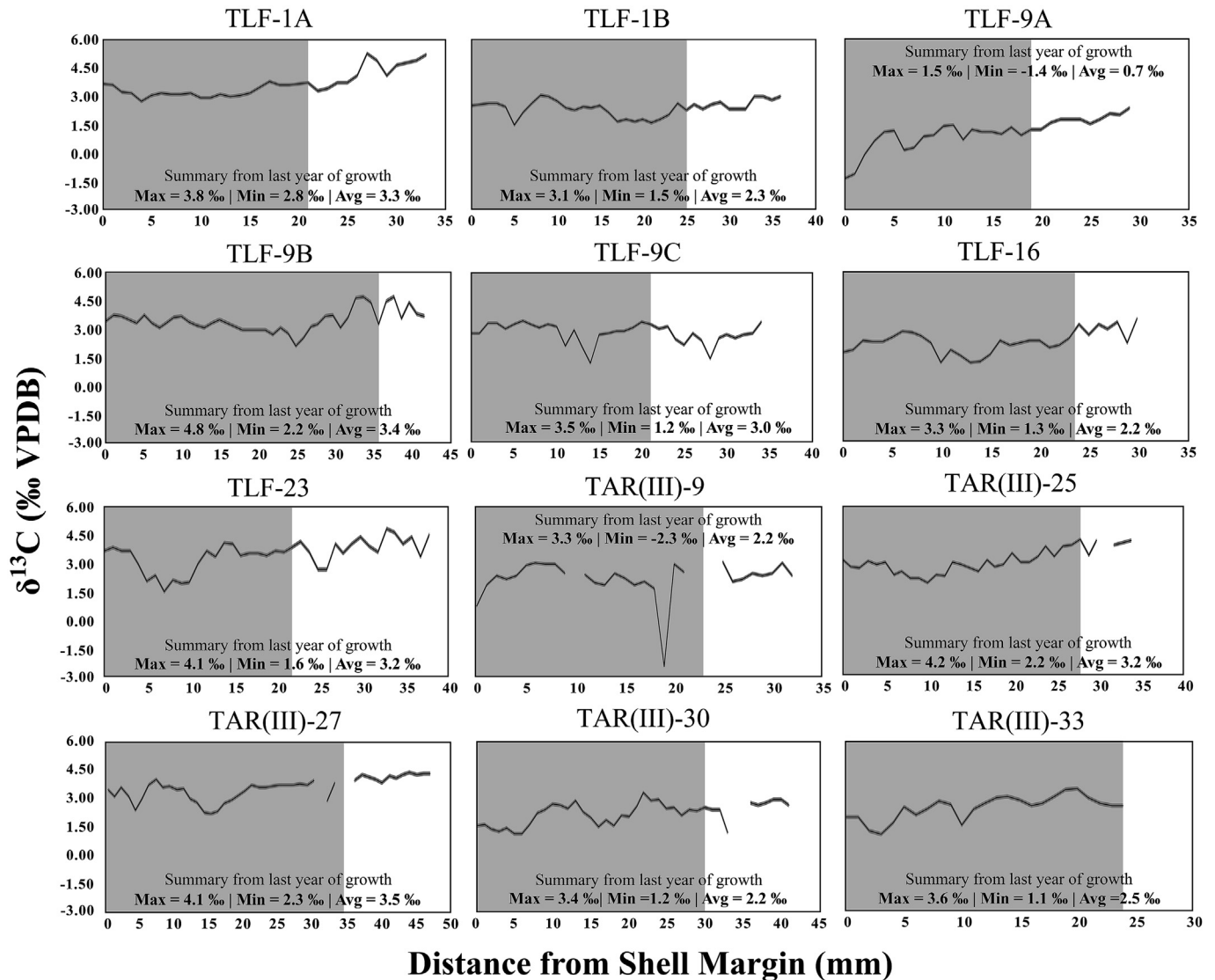


Fig. 6. Observed $\delta^{13}\text{C}$ values from shells retrieved from archaeological sites spanning the MCA in the Canary Islands. The light gray box depicts the last year of growth, as defined by summer and winter SSTs (Fig. 4). The dark gray error envelope around the data corresponds to the range of analytical error ($\pm 0.1\text{‰}$).

value across the water column of $0.83 \pm 0.19\text{‰}$. Consequently, it is possible that vertically displaced water masses could be characterized by a $\delta^{18}\text{O}$ signal that deviates by up to $\pm 0.2\text{‰}$ from the assumed value of 0.8‰ used in the SST calculations in this research. This accounts for a potential error envelope of $\pm 0.8\text{ °C}$ around the reconstructed MCA temperatures. To compare the influence of differing $\delta^{18}\text{O}_{\text{seawater}}$ values on the reconstructed SSTs from each archaeological site we generated additional violin plots as seen in Fig. 8. To verify the statistical validity of the differing offset between modern and ancient reconstructed SSTs we conducted additional Wilcoxon Rank-Sum tests. For these additional tests, we recalculated estimated SSTs from the archaeological shells using the endmember $\delta^{18}\text{O}_{\text{seawater}}$ values (0.6‰ and 1.0‰) and then compared them to the estimated modern SSTs (calculated using the observed $\delta^{18}\text{O}_{\text{seawater}}$ value of 0.8‰ from Parker et al., 2017). The modern and ancient reconstructed SSTs are significantly different (Wilcoxon Rank-Sum test, $P < .05$), even considering the $\pm 0.2\text{‰}$ uncertainty envelope surrounding the ancient $\delta^{18}\text{O}_{\text{seawater}}$ value. Consequently, we can reasonably infer that the increased $\delta^{18}\text{O}_{\text{shell}}$ values observed during shells spanning the MCA are directly

attributable to a cooling of the ambient seawater by $1.0\text{--}2.6\text{ °C}$, as the other potential impacts on $\delta^{18}\text{O}_{\text{shell}}$ values (e.g. isotope effects, seasonality) are negligible in this case study.

Carbon isotope ratios are also influenced by multiple biochemical and physical processes, including (1) kinetic isotope effects; (2) metabolic isotope effects; (3) reproduction; and (4) $\delta^{13}\text{C}_{\text{DIC}}$ values of the ambient seawater. Of these, kinetic isotope effects are unlikely to be a significant factor influencing $\delta^{13}\text{C}_{\text{shell}}$ values because there is no clear covarying relationship between $\delta^{13}\text{C}$ and $\delta^{18}\text{O}$ values.

Metabolic isotope effects occur when the shell uptakes respired carbon dioxide during the shell building process or in response to changes in pH, which results in a decrease in $\delta^{13}\text{C}$ values (McConnaughey, 1989b; McConnaughey and Gillikin, 2008; Swart, 1983). However, the amount of respired carbon utilized during calcification has been shown to remain consistent within a taxon (Fritz and Poplawski, 1974; Griffin and Druffel, 1989; Grossman, 1984; Paull et al., 1989; Spero and Lea, 1993). Thus, as modern shells are not expected to incorporate more respired carbon than their MCA counterparts, carbon isotope variations derived from

Estimated Final-Growth-Year $\delta^{13}\text{C}$ Values by Site

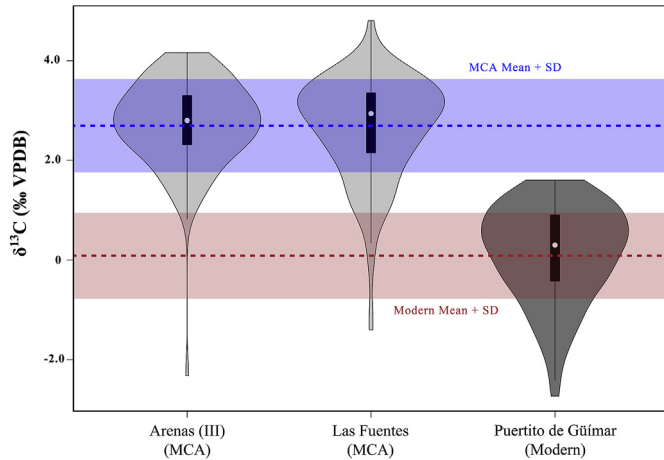


Fig. 7. Violin plot of all $\delta^{13}\text{C}_{\text{shell}}$ values retrieved from the final year of growth for all shells in this study. For comparison, the modern mean (0.1‰) and MCA mean (2.6‰) are denoted by a red and blue dashed line and bar, respectively. The width of the bar corresponds to the standard deviation of each mean (modern SD = 0.7‰ ; archaeological SD = 0.8‰). (For interpretation of the references to colour in this figure legend, the reader is referred to the Web version of this article.)

Estimated Final-Growth-Year SSTs at Differing $\delta^{18}\text{O}_{\text{seawater}}$ Values

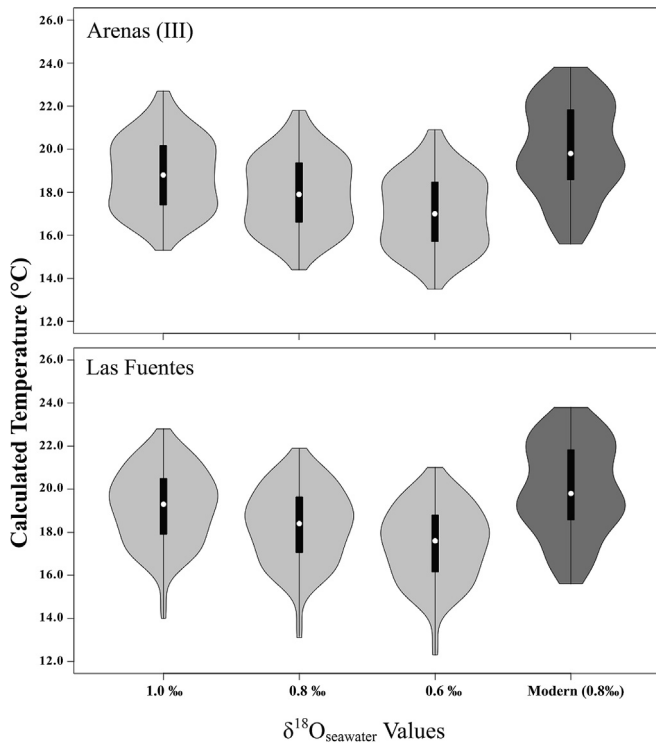


Fig. 8. Violin Plots comparing modern to ancient estimated SSTs from Arenas (III) and Las Fuentes using different plausible $\delta^{18}\text{O}_{\text{seawater}}$ values during the MCA.

respired CO_2 are unprovable.

Reproduction also influences shell $\delta^{13}\text{C}$ values as a result of potential growth cessation attributed to the deterioration of the gastropod's metabolism following periods of spawning in some gastropod genera (Nakashima et al., 2004). However, *Phorcus* at subtropical latitudes grow year-round, without significant growth cessation, and thus it has not been documented that reproduction

impacts the last-year shell growth cycle (Parker et al., 2017). Consequently, it is presumed that neither kinetic nor metabolic isotope effects, or reproduction, account for the 2.5‰ enrichment of ^{13}C in archaeological shells compared to modern ones. Thus, the $\delta^{13}\text{C}_{\text{shell}}$ values of *Phorcus atratus* from the Canary Islands are assumed to be primarily influenced by the $\delta^{13}\text{C}_{\text{DIC}}$ of the ambient seawater (McConnaughey and Gillikin, 2008).

No previous research has assessed the relationship between $\delta^{13}\text{C}_{\text{DIC}}$ and $\delta^{13}\text{C}_{\text{shell}}$ values in *P. atratus* from the Canaries. This work presents modern seawater $\delta^{13}\text{C}_{\text{DIC}}$ values and $\delta^{13}\text{C}_{\text{shell}}$ values to assess the linkages between DIC and shell carbon isotope budget. While this research does not present a comprehensive calibration of the carbon isotope systematics, here we present the first empirical dataset of $\delta^{13}\text{C}_{\text{DIC}}$ and $\delta^{13}\text{C}_{\text{shell}}$ values useful for a preliminary assessment. Data suggest that shells of *P. atratus* may underrepresent seawater $\delta^{13}\text{C}_{\text{DIC}}$ by $\sim 0.7\text{‰}$, pointing to a potential vital effect in the carbon isotope ratios of the shell. This offset was calculated by comparing mean modern $\delta^{13}\text{C}_{\text{shell}}$ values ($0.1 \pm 0.7\text{‰}$) with mean modern seawater $\delta^{13}\text{C}_{\text{DIC}}$ values ($0.9 \pm 0.2\text{‰}$). Surficial seawater $\delta^{13}\text{C}_{\text{DIC}}$ values measured in the Canary Islands are consistent with data reported by eGEOTRACES cruise GA03_e (Schlitzer, 2018). This cruise measured surface water $\delta^{13}\text{C}_{\text{DIC}}$ values that ranged from 0.6 to 1.1‰ between 27 and 29°N in the NE Atlantic Basin, approximately 500 km west of the Canary Islands (Quay and Wu, 2015). The magnitude of the offset in the carbon isotope ratios of seawater DIC and the shell is expected to remain consistent within the taxon, as has been shown in other mollusc species (e.g. Fenger et al., 2007; Land et al., 1977; Wefer and Berger, 1991). Accordingly, observed offsets in the carbon isotope ratios between the shell and seawater DIC are suspected to be constant for modern and MCA measured specimens.

5.2. Sea surface cooling during the MCA

Neither of the driving hypotheses of this research are supported by the empirical data: 1) seasonal amplitude of SST will be larger during the MCA compared to modern; and 2) mean annual SSTs will be similar to (within analytical error) today. The first hypothesis is not supported because both archaeological and modern shells exhibit a mean intra-annual SST range close to 5.5°C , indicating no significant difference in seasonal amplitude beyond analytical uncertainty. The second hypothesis is not supported because the mean SST from archaeological (MCA) shells ($18.2 \pm 0.7^\circ\text{C}$) is $\sim 2^\circ\text{C}$ lower than the mean SST from modern shells ($20.0 \pm 1.5^\circ\text{C}$), in contrast to model predictions by Mann et al. (2009). Measured shells indicate that both summer and winter SSTs in the Canary Islands were reduced during the MCA when compared to today.

A recent publication by Lüning et al. (2017) synthesizes data from 50 publications reporting MCA signals from 44 localities across Africa and Arabia, presenting data from terrestrial and marine proxy records at annual-to-multiannual resolution. In the location closest to the Canary Islands (Morocco), Lüning et al. (2017) compiled data from 10 publications featuring 9 proxy datasets. The terrestrial records come from a north-south transect through central Morocco, and the marine records are retrieved from two offshore clusters, two records from the Mediterranean Basin and three from the Cape Ghir upwelling system along the North Atlantic coastline. All terrestrial proxies and the two marine records located in the Mediterranean Basin indicate temperatures during the MCA that were slightly warmer than the present. In contrast, the marine records from the Atlantic coastline depict cooling trends (Lüning et al., 2017; McGregor et al., 2007; Morley et al., 2011) consistent with the data presented herein. The Atlantic records indicate cooling temperatures at the sea surface and bottom waters, which

McGregor et al. (2007) attributed to an intensification of the Cape Ghir upwelling cell.

The Cape Ghir upwelling system, located along the western Moroccan coastline, is one of the most persistent (year-round) upwelling zones along the African continent. Upwelling systems are often characterized by highly productive ecosystems fed by nutrient-rich bottom water drawn to the surface as a result of alongshore winds that force offshore Ekman transport of surface waters. Thus, changing wind patterns like the strengthening of the prevailing westerlies can result in the intensification of coastal upwelling as a result of enhanced flow within the subtropical gyre (Bakun, 1990; Desbiolles et al., 2014; Sydeman et al., 2014). In NW Africa, McGregor et al. (2007) argue that a rising contrast between terrestrial and oceanic surface temperatures drove stronger alongshore winds during the MCA, increasing the strength of the offshore upwelling system and subsequently cooling the entire water column. Their argument is supported by a concurrent rise in calcium deposition in one of their ocean sediment cores, interpreted as an increase in marine productivity and subsequent proliferation of calcium carbonate-bearing organisms (Lüning et al., 2017; McGregor et al., 2009, 2007). It is possible, therefore, that the depressed MCA SSTs presented in this study indicate that the zone of perpetual upwelling along the NW African coastline expanded during the MCA, bringing colder, nutrient-rich water as far west as the Canary Islands (13° W). Some research (e.g. McGregor et al., 2007) suggests that increased upwelling can be connected to changes in hemispheric-scale wind patterns, such as the strengthened westerly winds associated with the positive mode of the North Atlantic Oscillation (see Section 5.3 of this manuscript for additional discussion).

Previous studies have also observed an upwelling filament extending from the African coastline to SE Gran Canaria (150 km SE of the field sites in NW Tenerife) which actively exported upwelled water—characterized by low temperatures and high organic matter—seaward even in the absence of upwelling-favorable conditions in the Canary Islands (Barton et al., 2000, 1998; García-Muñoz et al., 2005). Specifically, Barton et al. (1998) reported that the filament manifested in SE Gran Canaria as a narrow tongue of seawater characterized by SSTs between 21.5 and 22 °C. This tongue surrounded a slightly warmer core but was still ~1 °C cooler than the surrounding seawater. Thus, it is possible that an intensification of the Cape Ghir upwelling zone could have brought colder water to the surface and could have transported it farther from the African continent in a filament that facilitated the oceanic cooling observed in Tenerife. Alternatively, it is possible the winds that drove enhanced coastal upwelling in NW Africa also drove smaller-scale, local upwelling along the north and west coast of Tenerife. Both of these scenarios adequately explain a ~2 °C decrease in SSTs during the MCA, but additional research would be necessary to discriminate between the presented scenarios.

Additional support for the upwelling scenario derives from our carbon isotope ratio datasets. The $\delta^{13}\text{C}_{\text{shell}}$ values reflect an enrichment in ^{13}C during the MCA when compared to the modern, which is likely representative of changing $\delta^{13}\text{C}_{\text{DIC}}$ values of the ambient seawater. Several environmental factors control the seawater $\delta^{13}\text{C}_{\text{DIC}}$ values including the oceanic Suess effect and the $\delta^{13}\text{C}$ values associated with nutrient-rich upwelled water and primary productivity. The first of these, the oceanic Suess effect, occurs in the modern oceans as a result of the anthropogenic burning of fossil fuels which release ^{13}C -depleted CO_2 into the atmosphere, resulting in lower atmospheric $\delta^{13}\text{C}$ values (Keeling, 1979). In turn, the lowered $\delta^{13}\text{C}$ values of atmospheric CO_2 is exchanged with oceanic surface waters, resulting in the lowering of modern $\delta^{13}\text{C}_{\text{DIC}}$ values (Böhm et al., 1996; Druffel and Suess, 1983; Keeling, 1979).

Several studies have quantified the oceanic Suess effect in seawater and biomineralized materials (e.g. scleractinian corals, bivalves, foraminifera) at a variety of localities (e.g. South China Sea, Atlantic Ocean, Southern Ocean) (Butler et al., 2009; Deng et al., 2017; King and Howard, 2004; Swart et al., 2010). These studies document that the Suess effect accounts for a 0.8–1.7‰ depression of modern (post-AD, 1900) seawater $\delta^{13}\text{C}_{\text{DIC}}$ values. While the magnitude of the oceanic Suess effect has not been quantified in the Canary Islands, Swart et al. (2010) comprehensively analyzed the oceanic Suess effect in both the Atlantic and Pacific basins. They reported that the magnitude of the oceanic Suess effect was greater in the Atlantic basin due to the relatively high rates of atmospheric recharge of CO_2 into surface waters when compared to the Pacific. Between 1900 and 2000, Swart et al. (2010) reported that the $\delta^{13}\text{C}_{\text{DIC}}$ values of Atlantic surface waters were lowered by approximately ~1‰. They also reported that, across the same 100 years, the $\delta^{13}\text{C}$ values of Atlantic sclerosponges dropped by a similar magnitude—approximately 0.75‰—at a rate of $-0.0074 \pm 0.0065\text{‰ yr}^{-1}$ (Swart et al., 2010). Estrella-Martínez et al. (2019b) found that in the North Atlantic basin the rate of change for the oceanic Suess effect was variable through time, but observed a net ~1.5‰ reduction of $\delta^{13}\text{C}_{\text{shell}}$ values in the bivalve *Arctica islandica* between 1850 and 2000 AD. The oceanic Suess effect is also more pronounced in subtropical latitudes due to the increased ventilation of the surface waters within the subtropical gyres (Eide et al., 2017; Swart et al., 2010). Considering the presented rate of change by Swart et al. (2010) for the Atlantic Basin, the $\delta^{13}\text{C}_{\text{DIC}}$ values of modern seawater in the Canary Islands could be reduced by ~1.0–1.5‰ when compared to pre-1900 values. In the present study, we adopted the most conservative estimates and assume that up to 1.5‰ of modern $\delta^{13}\text{C}_{\text{shell}}$ values to be attributable to the oceanic Suess effect. Interestingly, after taking into account a 1.5‰ decrease related to the Suess effect, MCA $\delta^{13}\text{C}_{\text{shell}}$ values remain ~1‰ higher than modern shells, suggesting that changes in oceanic upwelling and primary productivity must also play a role.

Coastal upwelling brings nutrient-rich water from the deep ocean to the surface, and this inflowing water is isotopically depleted in ^{13}C due to the oxidation of organic matter (Bakun, 1990; Kroopnick, 1974; Sharp, 2017). Thus, the $\delta^{13}\text{C}_{\text{DIC}}$ value of water in upwelling zones is continuously replaced with water characterized by more negative values. The upwelled water, rich in nutrients such as nitrogen and phosphorus, can also lead to high primary productivity in the photic zone. Photosynthetic organisms (i.e. phytoplankton) preferentially uptake ^{12}C during metabolic processes, thus enriching the remaining ambient seawater DIC with respect to ^{13}C (Sharp, 2017; Steens et al., 1992). Accordingly, upwelling and primary productivity have opposing effects on the $\delta^{13}\text{C}_{\text{DIC}}$ value of seawater, but typically occur in conjunction with one another. The skeletons of calcium carbonate-bearing organisms utilize ambient $\delta^{13}\text{C}_{\text{DIC}}$ during calcification, and accordingly $\delta^{13}\text{C}_{\text{shell}}$ values may provide insight into the relative dominance of these two factors (Poulain et al., 2010).

In the present study, the $\delta^{13}\text{C}$ values of archaeological shells display a ~2.5‰ increase when compared to the modern shells, of which ~1.5‰ can be attributed to the oceanic Suess effect. This finding implies that the increased $\delta^{13}\text{C}_{\text{DIC}}$ values associated with primary productivity narrowly outweighed the decreased $\delta^{13}\text{C}$ values associated with upwelled waters during the MCA, resulting in a slight overall net increase in $\delta^{13}\text{C}_{\text{DIC}}$ values in the surface waters inhabited by *Phorcus atratus*. Peeters et al. (2002) encountered an increase in $\delta^{13}\text{C}$ values in foraminiferal tests from upwelling zones in the Arabian sea, while Tao et al. (2013) reported no significant difference in gastropod shell $\delta^{13}\text{C}$ values between upwelling and non-upwelling zones along the Pacific coastline of Central America. Accordingly, while it is possible that higher $\delta^{13}\text{C}$ values of the

sampled *P. atratus* shells reflect high primary productivity associated with upwelling, additional time series analysis of modern and ancient $\delta^{13}\text{C}_{\text{shell}}$ values would be necessary to constrain and test the relative influences of upwelling and primary production on the $\delta^{13}\text{C}_{\text{shell}}$ values of *P. atratus*.

5.3. Implications for the NAO during the MCA

The results of our study indicate a possible increase in the intensity of upwelling in northwest Africa during the middle and late MCA, which in turn suggests a positive mode of the NAO. The NAO is the primary synoptic mode of atmospheric circulation in the North Atlantic, and is driven by the difference in pressure at sea level between the Azores high pressure system and the Icelandic low pressure system (Hurrell et al., 2003; NOAA, 2018). The interaction between these pressure systems impacts the strength and direction of the westerly winds (Hurrell et al., 2003). A positive (negative) NAO index is characterized by a greater-than-average (smaller-than-average) pressure differential and strengthened (weakened) westerlies (George and Saunders, 2001; NOAA, 2018). Global winds, such as the prevailing westerlies, exert wind stress on underlying surficial oceanwater and are part of the mechanism (in combination with the Coriolis effect) that drives the generation and sustenance of oceanic gyres including the North Atlantic Subtropical Gyre (NASG) (Hassan, 1950). Thus, strengthened prevailing westerlies during years with a positive NAO index are likely to drive an acceleration and strengthening of NASG circulation. A strengthened NASG is also associated with enhanced upwelling in NW Africa due to greater offshore Ekman transport driven by stronger along-shore winds and surface currents (Hagen, 2001). Consequently, enhanced upwelling in NW Africa can be indicative of a positive NAO index. The data presented here from the Canary Islands supports an increase in upwelling strength during the MCA, and thus also indicates the possible presence of a positive mode of the NAO during the MCA.

The relationship between the NAO and upwelling has been studied before; however, there is still much debate regarding the role the NAO may play in the modulation of the upwelling regimes of Europe and Northwest Africa. In support of the NAO/upwelling relationship, McGregor et al. (2007) argue that diminishing NAO indices in the late 20th century, coupled with constant Cape Ghir upwelling, indicated a loose connection between the NAO and upwelling in NW Africa. Conversely, Narayan et al. (2010) concluded that the connection between the NAO and upwelling in NW Africa was ambiguous, and there was no conclusive evidence that the NAO impacted NW African upwelling. Additional research lends support for the connection between the NAO and upwelling in Europe and Africa (Bode et al., 2009; deCastro et al., 2008; Lehmann et al., 2002), but all research indicates that coastal upwelling is driven by an interconnected range of factors that are inclusive of, but not limited to, the NAO.

NAO variability is, however, known to be linked to precipitation patterns in Europe and North Africa, and thus the NAO index can be approximated through analysis of precipitation and drought proxies. Trouet et al. (2009) used records retrieved from Scotland and Morocco to establish high- and low-latitude endmember precipitation values for the NAO dipole. The authors concluded that the MCA was characterized by a persistently positive mode of the NAO. They further proposed that atmospheric circulation variance associated with the positive NAO index were likely coupled with La Niña-like conditions. Other studies have correlated La Niña-like conditions with the strengthening of the Atlantic trade winds and subsequent enhancement of upwelling-favorable conditions in the subtropical Atlantic (Roy and Reason, 2001; Trouet et al., 2009).

These interpretations lend support to the interrelationship between NW African upwelling and a positive mode of the NAO.

Several proxy datasets and model results investigating other telltale NAO parameters (e.g. low temperatures in Greenland, warm temperatures in Northeastern Europe) during the MCA do not uniformly support the interpretation of a positive mode of the NAO (Gómez-Navarro and Zorita, 2013; Lehner et al., 2012; Ortega et al., 2014). Of these, Lehner et al. (2012) were unable to reconstruct a persistently positive NAO during the MCA using coupled general circulation models. However, the multi-model approach utilized by Ortega et al. (2014) demonstrated agreement with some of the NAO indices reported by Trouet et al. (2009) but still pointedly disagreed with the positive mode of the NAO during the early and middle MCA. Instead, Ortega et al. (2014) argues that a positive mode of the NAO manifested later, during the 13th and 14th centuries. Therefore, while both Trouet et al. (2009) and Ortega et al. (2014) indicate a transition to a positive NAO index by the latest portion of the MCA, they disagree on the timing of this transition.

Our data also support a shift to a positive NAO phase by the end of the MCA, but the limitations of our chronological data preclude a robust interpretation of the timing of this transition. The 2σ radiocarbon ages for archaeological shells in this study range from 900 to 1520 cal yrs AD, although most shells from both sites have median probability ages between 1090 and 1350 cal yrs AD. Therefore, while most archaeological shells at both sites likely derive from the middle or late MCA, some shells could have grown as late as 1520 AD. However, this knowledge gap in the early MCA is addressed by Surge and Barrett (2012) through the use of SST time-series analysis of *Patella vulgata* from the Orkney archipelago, Scotland.

Surge and Barrett (2012) argue that the beginning of the MCA (around 900 AD) was characterized by a negative NAO index, as supported by colder winters and increased seasonality in Scotland. Additionally, they suggest that closer investigation of the data from Trouet et al. (2009) demonstrates lower NAO indices in the earliest part of their record, which is consistent with Surge and Barrett's (2012) interpretation of a negative NAO index in the early MCA. Their study, combined with our data, the findings of Trouet et al. (2009), and the models generated by Ortega et al. (2014) support a shift of the NAO index from a negative to a positive phase during the middle of the MCA, which then remained consistently positive through the end of the MCA and into the 14th and (possibly) 15th centuries AD. While the timing of this transition is still up for debate, results available to date indicate that the MCA was impacted by the interplay of a wide range of contrasting and compounding climatic phenomena (i.e., Atlantic Oscillation, Atlantic Meridional Overturning Circulation, El Niño-Southern Oscillation) across multiple centuries in the North Atlantic (Cohen and Barlow, 2005; Trouet et al., 2012; Wanamaker et al., 2012).

6. Conclusion

High-resolution $\delta^{18}\text{O}$ and $\delta^{13}\text{C}$ time-series spanning the MCA in the subtropical eastern North Atlantic Ocean were retrieved for the first time using serial sampling of radiocarbon-dated *Phorcus atratus* shells preserved in archaeological sites on Tenerife, Canary Islands. Modern shells were also serially sampled, and the oxygen isotope data from both archaeological and modern shells were used to reconstruct paleotemperatures during the MCA. Results indicate that the mean SST from shells spanning the MCA was 18.2 ± 0.7 °C, while SST from modern shells was 20.0 ± 1.5 °C. Observed seasonality was $\sim 5.5 \pm \sim 1$ °C for both modern and archaeological shells. Recorded summer and winter SSTs in the Canary Islands were reduced by ~ 2 °C in shells spanning the MCA compared to

those from the modern.

The documented cooling in the Canary Islands is greater than expected from published predictive climate models and may be explained by enhanced upwelling during the MCA off the coast of Northwest Africa. It is unclear, however, if the upwelling was generated locally (near the NW coast of Tenerife) or if the shells are recording signals from the further afield Cape Ghir upwelling zone (NW Africa), centered ~400 km east of the field sites. Additional data from other parts of Tenerife and other islands in the archipelago would help constrain and clarify the relative impact of the Cape Ghir upwelling zone compared to the localized upwelling scenario. The intensified upwelling scenario during the MCA is supported by the $\delta^{13}\text{C}_{\text{shell}}$ data (MCA: $2.6 \pm 0.8\%$ and modern: $0.1 \pm 0.7\%$). Increased MCA $\delta^{13}\text{C}_{\text{shell}}$ values likely reflect high primary productivity, which can occur in conjunction with upwelling zones containing ^{13}C -enriched ambient seawater DIC. However, an observed ~0.7‰ offset between modern $\delta^{13}\text{C}_{\text{shell}}$ and $\delta^{13}\text{C}_{\text{DIC}}$ values was observed, and ongoing investigation is underway to further quantify and characterize the incorporation of seawater DIC and respired carbon into the *P. atratus* aragonitic shell layer.

The establishment of upwelling-favorable conditions, which we hypothesize to have occurred during the middle to late MCA in the Canary Islands, is potentially indicative of a positive index of the North Atlantic Oscillation. This research, in conjunction with other published work, suggests a transition into the positive mode of the NAO during the middle to late MCA that could have extended beyond the end of the MCA into the 14th and 15th centuries AD. However, continued research and additional high-resolution proxy data are much needed to investigate the intricate teleconnections between global and hemispheric climate mechanisms and oceanic phenomena, particularly in relationship to the MCA.

Declaration of competing interest

The authors declare that they have no known competing financial interests or personal relationships that could have appeared to influence the work reported in this paper.

Acknowledgements

This research was funded by National Science Foundation (NSF) Grant No. 1802153 awarded to Y.Y. and D.S. Additional support was provided by the Paleontological Society (PS) Ellis L. Yochelson Award, Geological Society of America (GSA) Graduate Research Grant Nos. 11303–16 and 11625–17, and a 2016 SEPM Foundation Student Assistance Grant, all awarded to W.P. This material is based upon work supported by the Graduate School Dean's Dissertation Completion Fellowship at the University of Cincinnati, and the NSF Graduate Research Fellowship Program Grant No.1610397, both awarded to W.P. Any opinions, findings, and conclusions or recommendations expressed in this material are those of the author(s) and do not necessarily reflect the views of the National Science Foundation or the University of Cincinnati. The authors would like to thank Mallin Blaxall (University of Cincinnati) for her assistance with sample collection, and Drs. Adriane Lam (SUNY Binghamton) and Aaron Diefendorf (University of Cincinnati) for their constructive intellectual discussions. We would also like to thank three anonymous reviewers whose constructive feedback increased the quality and clarity of this publication.

Appendix A. Supplementary data

Supplementary data to this article can be found online at <https://doi.org/10.1016/j.quascirev.2020.106635>.

References

- Adler, D., Kelly, S.T., 2018. *Vioplot: Violin Plot. R Package, version 0.3.2*.
- Agencia Estatal de Meteorología, 2020. AEMET climate atlas [WWW Document]. URL: http://www.aemet.es/en/serviciosclimaticos/datosclimatologicos/atlas_climatico.
- Ancochea, E., Brändle, J.L., Huertas, M.J., Cubas, C.R., Hernán, F., 2003. The felsic dikes of La Gomera (Canary Islands): identification of cone sheet and radial dike swarms. *J. Volcanol. Geoth. Res.* 120, 197–206. [https://doi.org/10.1016/S0377-0273\(02\)00384-0](https://doi.org/10.1016/S0377-0273(02)00384-0).
- Andrus, C.F.T., 2011. Shell midden sclerochronology. *Quat. Sci. Rev.* 30, 2892–2905. <https://doi.org/10.1016/j.quascirev.2011.07.016>.
- Arnay-de-la-Rosa, M., Gámez-Mendoza, A., Navarro-Mederos, J.F., Hernández-Marrero, J.C., Fregel, R., Yanes, Y., Galindo-Martín, L., Romanek, C.S., González-Reimers, E., 2009. Dietary patterns during the early prehispanic settlement in La Gomera (Canary Islands). *J. Archaeol. Sci.* 36 <https://doi.org/10.1016/j.jas.2009.05.018>, 1972–1981.
- Arnay-de-la-Rosa, M., González-Reimers, E., Yanes, Y., Velasco-Vázquez, J., Romanek, C.S., Noakes, J.E., 2010. Paleodietary analysis of the prehistoric population of the Canary Islands inferred from stable isotopes (carbon, nitrogen and hydrogen) in bone collagen. *J. Archaeol. Sci.* 37, 1490–1501. <https://doi.org/10.1016/j.jas.2010.01.009>.
- Aufderheide, A.C., Rodríguez-Martín, C., Estevez-Gonzalez, F., Torbenson, M., 1992. Chemical dietary reconstruction of Tenerife's guanche diet using skeletal trace element content. *Actas del I Congr. Int. Estud. sobre Momias* 1, 33–40.
- Bakun, A., 1990. Global climate change and intensification of coastal ocean upwelling. *Science* 84 247, 198–201. <https://doi.org/10.3354/meps274235>.
- Barton, E.D., Aristegui, J., Tett, P., Canton, M., García-Braun, J., Hernández-León, S., Nykjaer, L., Almeida, C., Almunia, J., Ballesteros, S., Basterretxea, G., Escanez, J., García-Weill, L., Hernández-Guerra, A., López-Laatzén, F., Molina, R., Montero, M.F., Navarro-Peréz, E., Rodríguez, J.M., Van Lenning, K., Vélez, H., Wild, K., 1998. The transition zone of the Canary Current upwelling region. *Prog. Oceanogr.* 41, 455–504. [https://doi.org/10.1016/S0079-6611\(98\)00023-8](https://doi.org/10.1016/S0079-6611(98)00023-8).
- Barton, E.D., Basterretxea, G., Flament, P., Mitchelson-Jacob, E.G., Jones, B., Affstegui, J., Herrera, F., 2000. Lee region of gran Canaria. *J. Geophys. Res.* 105 (17), 173–179.
- Bellard, C., Bertelsmeier, C., Leadley, P., Thuiller, W., Courchamp, F., 2012. Impacts of climate change on the future of biodiversity. *Ecol. Lett.* 15, 365–377. <https://doi.org/10.1111/j.1461-0248.2011.01736.x>.
- Berger, A., 2013. *Milankovitch and Climate: Understanding the Response to Astronomical Forcing*. Springer Science & Business Media.
- Bode, A., Alvarez-Ossorio, M.T., Cabanas, J.M., Miranda, A., Varela, M., 2009. Recent trends in plankton and upwelling intensity off Galicia (NW Spain). *Prog. Oceanogr.* 83, 342–350. <https://doi.org/10.1016/j.pocean.2009.07.025>.
- Böhm, F., Joachimski, M.M., Lehnert, H., Morgenroth, G., Kretschmer, W., Vacelet, J., Dullo, W.C., 1996. Carbon isotope records from extant Caribbean and South Pacific sponges: evolution of $\delta^{13}\text{C}$ in surface water DIC. *Earth Planet Sci. Lett.* 139, 291–303. [https://doi.org/10.1016/0012-821x\(96\)00006-4](https://doi.org/10.1016/0012-821x(96)00006-4).
- Bueno, C., Carta, J.A., 2006. Wind powered pumped hydro storage systems, a means of increasing the penetration of renewable energy in the Canary Islands. *Renew. Sustain. Energy Rev.* 10, 312–340. <https://doi.org/10.1016/j.rser.2004.09.005>.
- Bush, S.L., Santos, G.M., Xu, X., Southon, J.R., Thiagarajan, N., Hines, S.K., Adkins, J.F., 2013. Simple, Rapid, and Cost Effective: a Screening Method for Analysis of Small Carbonate Samples 14 C 55, pp. 631–640.
- Butler, P.G., Scourse, J.D., Richardson, C.A., Wanamaker, A.D., Bryant, C.L., Bennell, J.D., 2009. Continuous marine radiocarbon reservoir calibration and the 13C Suess effect in the Irish Sea: results from the first multi-centennial shell-based marine master chronology. *Earth Planet Sci. Lett.* 279, 230–241. <https://doi.org/10.1016/j.epsl.2008.12.043>.
- Cobb, K.M., Charles, C.D., Cheng, H., Edwards, R.L., 2003. El Niño/Southern Oscillation and tropical Pacific climate during the last millennium. *Nature* 424, 271–276. <https://doi.org/10.1038/nature01779>.
- Cohen, J., Barlow, M., 2005. The NAO, the AO, and global warming: how closely related? *J. Clim.* 18, 4498–4513. <https://doi.org/10.1175/JCLI3530.1>.
- Colanese, A.C., Troelstra, S., Ziveri, P., Martini, F., Lo Vetro, D., Tommasini, S., 2009. Mesolithic shellfish exploitation in SW Italy: seasonal evidence from the oxygen isotopic composition of *Osilinus turbinatus* shells. *J. Archaeol. Sci.* 36, 1935–1944. <https://doi.org/10.1016/j.jas.2009.04.021>.
- Cronin, T.M., Hayo, K., Thunell, R.C., Dwyer, G.S., Saenger, C., Willard, D.A., 2010. The medieval climate anomaly and little ice age in Chesapeake bay and the north Atlantic Ocean. *Palaeogeogr. Palaeoclimatol. Palaeoecol.* 297, 299–310. <https://doi.org/10.1016/j.palaeo.2010.08.009>.
- Crowley, T., 2000. Causes of climate change over the past 1000 years. *Science* 84 289, 270–277. <https://doi.org/10.1126/science.289.5477.270>.
- Cullen, H.M., Demenocal, P.B., Hemming, S., Hemming, G., Brown, F.H., Guilderson, T., Sirocko, F., 2000. Climate change and the collapse of the Akkadian empire: evidence from the deep sea. *Geology* 28, 379–382. [https://doi.org/10.1130/0091-7613\(2000\)28<379:CCATCO>2.0.CO;2](https://doi.org/10.1130/0091-7613(2000)28<379:CCATCO>2.0.CO;2).
- Culleton, B.J., Kennett, D.J., Ingram, B.L., ERLANDSON, J.M., Southon, J.R., 2006. Intra-shell radiocarbon variability in marine mollusks. *Radiocarbon* 48, 387–400.
- deCastro, M., Gómez-Gesteira, M., Lorenzo, M.N., Alvarez, I., Crespo, A.J.C., 2008. Influence of atmospheric modes on coastal upwelling along the western coast of the Iberian Peninsula, 1985 to 2005. *Clim. Res.* 36, 169–179. <https://doi.org/10.3354/cr00742>.

- Deng, W., Chen, X., Wei, G., Zeng, T., Zhao, J.X., 2017. Decoupling of coral skeletal $\delta^{13}\text{C}$ and solar irradiance over the past millennium caused by the oceanic Suess effect. *Paleoceanography* 32, 161–171. <https://doi.org/10.1002/2016PA003049>.
- Desbiolles, F., Blanke, B., Bentamy, A., 2014. Short-term upwelling events at the western African coast related to synoptic atmospheric structures as derived from satellite observations. *J. Geophys. Res. Ocean.* 119, 461–483. <https://doi.org/10.1002/2013JC009278>.
- dos Santos, G.M., KCCAMS prep-laboratory personnel, 2018. W.M. Keck carbon cycle accelerator mass spectrometer, 2.15.20, [WWW Document]. URL <https://www.ess.uci.edu/group/ams/protocols>.
- Douglas, P.M.J., Pagani, M., Canuto, M.A., Brenner, M., Hodell, D.A., Eglinton, T.I., Curtis, J.H., 2015. Drought, agricultural adaptation, and sociopolitical collapse in the Maya Lowlands. *Proc. Natl. Acad. Sci. Unit. States Am.* 112, 5607–5612. <https://doi.org/10.1073/pnas.1419133112>.
- Drinkwater, K.F., Belgrano, A., Borja, A., Conversi, A., Edwards, M., Greene, C.H., Ottersen, G., Pershing, A.J., Walker, H., 2003. The response of marine ecosystems to climate variability associated with the north atlantic oscillation. *Geophys. Monogr.* 134, 211–234. <https://doi.org/10.1029/134GM01>.
- Druffel, E.M., Suess, H.E., 1983. On the radiocarbon record in banded corals: exchange parameters and net transport of ^{14}C between atmosphere and surface ocean. *J. Geophys. Res. Ocean.* 88, 1271–1280.
- Eide, M., Olsen, A., Ninnemann, U.S., Eldevik, T., 2017. A global estimate of the full oceanic ^{13}C Suess effect since the preindustrial. *Global Biogeochem. Cycles* 31, 492–514. <https://doi.org/10.1002/2016GB005472>.
- Estrella-Martínez, J., Ascough, P.L., Schöne, B.R., Scourse, J.D., Butler, P.G., 2019a. 8.2 ka event North Sea hydrography determined by bivalve shell stable isotope geochemistry. *Sci. Rep.* 9, 1–9. <https://doi.org/10.1038/s41598-019-43219-1>.
- Estrella-Martínez, J., Schöne, B.R., Thurstan, R.H., Capuzzo, E., Scourse, J.D., Butler, P.G., 2019b. Reconstruction of Atlantic herring (*Clupea harengus*) recruitment in the North Sea for the past 455 years based on the $\delta^{13}\text{C}$ from annual shell increments of the ocean quahog (*Arctica islandica*). *Fish Fish.* 20, 537–551. <https://doi.org/10.1111/faf.12362>.
- Fenger, T., Surge, D., Schöne, B., Milner, N., 2007. Sclerochronology and geochemical variation in limpet shells (*Patella vulgata*): a new archive to reconstruct coastal sea surface temperature. *G-cubed* 8. <https://doi.org/10.1029/2006GC001488>.
- Flores, Larruga, González, Hernández, Pinto, Cabrera, 2001. The origin of the canary island aborigines and their contribution to the modern population: a molecular genetics perspective. *Curr. Anthropol.* 42, 749. <https://doi.org/10.2307/3596575>.
- Fregel, R., Pestano, J., Arnay, M., Cabrera, V.M., Larruga, J.M., González, A.M., 2009. The maternal aborigine colonization of La Palma (Canary Islands). *Eur. J. Hum. Genet.* 17, 1314–1324. <https://doi.org/10.1038/ejhg.2009.46>.
- Friedman, I., O'Neil, J.R., 1977. *Data of Geochemistry: Compilation of Stable Isotope Fractionation Factors of Geochemical Interest*, vol. 440. US Government Printing Office.
- Friis-Christensen, E., Lassen, K., 1991. Length of the solar cycle: an indicator of solar activity closely associated with climate. *Science* 84 254, 698–700. <https://doi.org/10.1126/science.254.5032.698>.
- Fritz, P., Poplawski, S., 1974. ^{18}O and ^{13}C in the shells of freshwater molluscs and their environments. *Earth Planet Sci. Lett.* 24, 91–98. [https://doi.org/10.1016/0012-821X\(74\)90012-0](https://doi.org/10.1016/0012-821X(74)90012-0).
- Galván, B., Hernández, C., Velasco, J., Alberto, V., Borges, E., Barro, A., Larruga, A., 1999. Orígenes de Buenavista del Norte: de los primeros pobladores a los inicios de la colonización europea. *Ayunt. Buenavista del Norte*. St. Cruz Tenerife.
- García-Muñoz, M., Arístegui, J., Pelegrí, J.L., Antoranz, A., Ojeda, A., Torres, M., 2005. Exchange of carbon by an upwelling filament off Cape Ghir (NW Africa). *J. Mar. Syst.* 54, 83–95. <https://doi.org/10.1016/j.jmarsys.2004.07.005>.
- García Herrera, R., Gallego Puyol, D., Hernández Martín, E., Gimeno Presa, L., Ribera Rodríguez, P., 2001. Influence of the north atlantic oscillation on the precipitation in the canary islands. *J. Clim.* 14, 3889–3903.
- George, S.E., Saunders, M.A., 2001. North Atlantic Oscillation impact on tropical north Atlantic winter atmospheric variability. *Geophys. Res. Lett.* 28, 1015–1018. <https://doi.org/10.1029/2000GL012449>.
- Gómez-Navarro, J.J., Zorita, E., 2013. Atmospheric annular modes in simulations over the past millennium: No long-term response to external forcing. *Geophys. Res. Lett.* 40, 3232–3236. <https://doi.org/10.1002/grl.50628>.
- Gonfiantini, R., Stichler, W., Rozanski, K., 1995. *Standards and Intercomparison Materials Distributed by the International Atomic Energy Agency for Stable Isotope Measurements*.
- Graham, N.E., Ammann, C.M., Fleitmann, D., Cobb, K.M., Luterbacher, J., 2011. Support for global climate reorganization during the “medieval climate anomaly”. *Clim. Dynam.* 37, 1217–1245. <https://doi.org/10.1007/s00382-010-0914-z>.
- Granado, I., Caballero, P., 2001. Feeding rates of *Littorina striata* and *Ostilinus atratus* in relation to nutritional quality and chemical defenses of seaweeds. *Mar. Biol.* 138, 1213–1224. <https://doi.org/10.1007/s002270100544>.
- Griffin, S., Druffel, E.R.M., 1989. Sources of carbon to deep-sea corals. *Radiocarbon* 31, 533–543. <https://doi.org/10.1017/s003822200012121>.
- Grossman, E.L., 1984. Carbon isotopic fractionation in live benthic foraminifera-comparison with inorganic precipitate studies. *Geochem. Cosmochim. Acta* 48, 1505–1512. [https://doi.org/10.1016/0016-7037\(84\)90406-X](https://doi.org/10.1016/0016-7037(84)90406-X).
- Grossman, E.L., Ku, T.-L., 1986. Oxygen and carbon isotope fractionation in biogenic aragonite: temperature effects. *Chem. Geol. Isotop. Geosci. Sect.* 59, 59–74. [https://doi.org/10.1016/0168-9622\(86\)90057-6](https://doi.org/10.1016/0168-9622(86)90057-6).
- Hagen, E., 2001. Northwest African upwelling scenario. *Oceanol. Acta* 24, S113–S128. [https://doi.org/10.1016/s0399-1784\(00\)01110-5](https://doi.org/10.1016/s0399-1784(00)01110-5).
- Harley, C.D.G., Randall Hughes, A., Hultgren, K.M., Miner, B.G., Sorte, C.J.B., Thornber, C.S., Rodriguez, L.F., Tomanek, L., Williams, S.L., 2006. The impacts of climate change in coastal marine systems: climate change in coastal marine systems. *Ecol. Lett.* 9, 228–241. <https://doi.org/10.1111/j.1461-0248.2005.00871.x>.
- Hassan, E.M., 1950. On the wind driven ocean circulation. *Deep Sea Res.* [https://doi.org/10.1016/S0146-6291\(58\)80006-5](https://doi.org/10.1016/S0146-6291(58)80006-5).
- Hintze, J.L., Nelson, R.D., 1998. Violin plots: a box plot-density trace synergism statistical computing and graphics violin plots: a box plot-density trace synergism. *Source Am. Stat.* 52, 181–184.
- Hurrell, J.W., Kushnir, Y., Ottersen, G., Visbeck, M., 2003. An overview of the north atlantic oscillation. *Geophys. Monogr.* 134, 1–35. <https://doi.org/10.1029/134GM01>.
- Japan Meteorological Agency, 2006. Characteristics of global sea surface temperature analysis data (COBE-SST) for climate use. In: *Monthly Report on Climate System Separated*, vol. 12, p. 116.
- Jones, P.D., Mann, M.E., 2004. Climate over past millennia. *Rev. Geophys.* 42 <https://doi.org/10.1029/2003RG000143>.
- Keeling, C.D., 1979. The Suess effect: ^{13}C Carbon- ^{14}C Carbon interrelations. *Environ. Int.* 2, 229–300. [https://doi.org/10.1016/0160-4120\(79\)90005-9](https://doi.org/10.1016/0160-4120(79)90005-9).
- King, A.L., Howard, W.R., 2004. Planktonic foraminiferal $\delta^{13}\text{C}$ records from Southern Ocean sediment traps: new estimates of the oceanic Suess effect. *Global Biogeochem. Cycles* 18, 1–16. <https://doi.org/10.1029/2003GB002162>.
- Kowalewski, M., Casebolt, S., Hua, Q., Whitacre, K.E., Kaufman, D.S., Kosnik, M.A., 2017. One fossil record, multiple time resolutions: disparate timeaveraging of echinoids and mollusks on a Holocene carbonate platform. *Geology* 46, 51–54. <https://doi.org/10.1130/G39789.1>.
- Kroopnick, P., 1974. Correlations between ^{13}C and ^{18}O in surface waters and atmospheric CO_2 . *Earth Planet Sci. Lett.* 22, 397–403.
- Kushnir, Y., Wallace, J.M., 1989. Low-frequency variability in the northern hemisphere winter: geographical distribution, structure and time-scale dependence. *J. Atmos. Sci.* 46, 3122–3143.
- LaMarche, V.C., 1974. Paleoclimatic Inferences from Long Tree-Ring Records: intersite comparison shows climatic anomalies that may be linked to features of the general circulation. *Science* (80-) 183, 1043–1048.
- Lamb, H.H., 1965. The early medieval warm epoch and its sequel. *Palaeogeogr. Palaeoclimatol. Palaeoecol.* 1, 13–37.
- Land, L.S., Lang, J.C., Barnes, D.J., 1977. On the stable carbon and oxygen isotopic composition of some shallow water, ahermatypic, scleractinian coral skeletons. *Geochem. Cosmochim. Acta* 41, 169–172. [https://doi.org/10.1016/0016-7037\(77\)90197-1](https://doi.org/10.1016/0016-7037(77)90197-1).
- Lehmann, A., Krauss, W., Hinrichsen, H.H., 2002. Effects of remote and local atmospheric forcing on circulation and upwelling in the Baltic Sea. *Tellus Ser. A Dyn. Meteorol. Oceanogr.* 54, 299–316. <https://doi.org/10.1034/j.1600-0870.2002.00289.x>.
- Lehner, F., Raible, C.C., Stocker, T.F., 2012. Testing the robustness of a precipitation proxy-based North Atlantic Oscillation reconstruction. *Quat. Sci. Rev.* 45, 85–94. <https://doi.org/10.1016/j.quascirev.2012.04.025>.
- Lüning, S., Gaika, M., Vahrenholt, F., 2017. Warming and cooling: the medieval climate anomaly in Africa and Arabia. *Paleoceanography* 32, 1219–1235. <https://doi.org/10.1002/2017PA003237>.
- Maca-Meyer, N., Arnay, M., Rando, J.C., Flores, C., González, A.M., Cabrera, V.M., Larruga, J.M., 2004. Ancient mtDNA analysis and the origin of the Guanches. *Eur. J. Hum. Genet.* 12, 155–162. <https://doi.org/10.1038/sj.ejhg.5201075>.
- Macías, A.G., 2017. *Estructura poblacional de los moluscos gastrópodos Phorcus sauciatu y P. atratus en el litoral de Tenerife (In Spanish)*.
- Mann, M.E., 2007. Climate over the past two millennia. *Annu. Rev. Earth Planet Sci.* 35, 111. <https://doi.org/10.1146/annurev.earth.35.031306.140042>.
- Mann, M.E., Zhang, Z., Rutherford, S., Bradley, R.S., Hughes, M.K., Shindell, D., Ammann, C., Faluvegi, G., Ni, F., 2009. Global signatures and dynamical origins of the little ice age and medieval climate anomaly. *Science* 84 326, 1256–1260. <https://doi.org/10.1126/science.1166349>.
- Mannino, M.A., Thomas, K.D., Leng, M.J., Piperno, M., Tusa, S., Tagliacozzo, A., 2007. Marine resources in the mesolithic and neolithic at the grotta Dell’Uzzo (sicily): evidence from isotope analyses of marine shells*. *Archaeometry* 49, 117–133. <https://doi.org/10.1111/j.1475-4754.2007.00291.x>.
- Marzol, M.V., 2008. Temporal characteristics and fog water collection during summer in Tenerife (Canary Islands, Spain). *Atmos. Res.* 87, 352–361. <https://doi.org/10.1016/j.atmosres.2007.11.019>.
- McConnaughey, T., 1989a. ^{13}C and ^{18}O isotopic disequilibrium in biological carbonates: I. Patterns. *Geochem. Cosmochim. Acta* 53, 151–162.
- McConnaughey, T., 1989b. ^{13}C and ^{18}O isotopic disequilibrium in biological carbonates: II. In vitro simulation of kinetic isotope effects. *Geochem. Cosmochim. Acta* 53, 163–171.
- McConnaughey, T.A., Gillikin, D.P., 2008. Carbon isotopes in mollusk shell carbonates. *Geo Mar. Lett.* 28, 287–299. <https://doi.org/10.1007/s00367-008-0116-4>.
- McGregor, H.V., Dima, M., Fischer, H.W., Mulitza, S., 2007. Rapid 20th-century increase in coastal upwelling off northwest Africa. *Science* 84 315, 637–639. <https://doi.org/10.1126/science.1134839>.
- McGregor, H.V., Dupont, L., Stuu, J.B.W., Kuhlmann, H., 2009. Vegetation change, goats, and religion: a 2000-year history of land use in southern Morocco. *Quat. Sci. Rev.* 28, 1434–1448. <https://doi.org/10.1016/j.quascirev.2009.02.012>.
- Mercer, J., 1980. *The Canary Islanders: their prehistory, conquest, and survival*. Collings.
- Mesa Hernández, E.M., 2008. *Las arqueomalacofaunas en contextos prehistóricos de Tenerife (In Spanish)*. XVII Coloq. Hist. Canar. 414–452.

- Mesa Hernández, E.M., 2006. Los Aborígenes Y El Mar: Los Concheros De Canarias. Universidad de la Laguna (In Spanish).
- Monges Soares, A.M., 1993. Isotope techniques in the study of past and current environmental changes in the hydrosphere and atmosphere. In: Proceedings of Vienna. IAEA-SM, pp. 471–485.
- Morley, A., Schulz, M., Rosenthal, Y., Mulitza, S., Paul, A., Rühlemann, C., 2011. Solar modulation of North Atlantic central Water formation at multidecadal time-scales during the late Holocene. *Earth Planet Sci. Lett.* 308, 161–171. <https://doi.org/10.1016/j.epsl.2011.05.043>.
- Nakashima, R., Suzuki, A., Watanabe, T., 2004. Life history of the Pliocene scallop *Fortipecten*, based on oxygen and carbon isotope profiles. *Palaeogeogr. Palaeoclimatol. Palaeoecol.* 211, 299–307. <https://doi.org/10.1016/j.palaeo.2004.05.011>.
- Narayan, N., Paul, A., Mulitza, S., Schulz, M., 2010. Trends in coastal upwelling intensity during the late 20th century. *Ocean Sci.* 6, 815–823. <https://doi.org/10.5194/os-6-815-2010>.
- Navarro-Pérez, E., Barton, E.D., 2001. Seasonal and interannual variability of the canary current. *Sci. Mar.* 65, 205–213. <https://doi.org/10.3989/scimar.2001.65s1205>.
- Navarro Mederos, J.F., Hernández Gómez, C.M., Barro Rois, A., Borges Domínguez, E., Hernández Marrero, J.C., Alberto Barroso, V., 2001. La Fortaleza de Chipude y los concheros de Arguamul al cabo de tres décadas. Viejos problemas, nuevas interpretaciones. (In Spanish). *Spal* 10, 327–341.
- Ndeye, M., 2008. Marine reservoir ages in northern Senegal and Mauritania coastal waters. *Radiocarbon* 50, 281–288.
- New, E., Yanes, Y., Cameron, R.A.D., Miller, J.H., Teixeira, D., Kaufman, D.S., 2019. Amino-chronology and time-averaging of Quaternary land snail assemblages from colluvial deposits in the Madeira Archipelago (Portugal). *Quat. Res.*
- NOAA, 2018. North Atlantic oscillation (NAO) [WWW document]. NOAA teleconnections. <https://www.ncdc.noaa.gov/teleconnections/nao/>.
- Ortega, P., Lehner, F., Casado, M., Swingedouw, D., Masson-Delmotte, V., Yiou, P., Raible, C., 2014. A multi-proxy model-tested NAO reconstruction for the last millennium. *EGU Gen. Assem. Conf. Abstr.* 16.
- Otto, R., Krüsi, B.O., Burga, C.A., Fernández-Palacios, J.M., 2006. Old-field succession along a precipitation gradient in the semi-arid coastal region of Tenerife. *J. Arid Environ.* 65, 156–178. <https://doi.org/10.1016/j.jaridenv.2005.07.005>.
- Parker, W.G., Yanes, Y., Mesa Hernández, E., Hernández Marrero, J.C., Pais, J., Soto Contreras, N., Surge, D., 2018. Shellfish exploitation in the western canary islands over the last two millennia. *Environ. Archaeol.* 1–23. <https://doi.org/10.1080/14614103.2018.1497821>.
- Parker, W.G., Yanes, Y., Mesa Hernández, E., Hernández Marrero, J.C., Pais, J., Surge, D., 2019. Scale of Time-Averaging in Archaeological Shell Middens from the Canary Islands. *The Holocene* In Press, pp. 1–14. <https://doi.org/10.1177/0959683619883020>.
- Parker, W.G., Yanes, Y., Surge, D., Mesa-Hernández, E., 2017. Calibration of the oxygen isotope ratios of the gastropods *Patella candei crenata* and *Phorcus atratus* as high-resolution paleothermometers from the subtropical eastern Atlantic Ocean. *Palaeogeogr. Palaeoclimatol. Palaeoecol.* 487, 251–259. <https://doi.org/10.1016/j.palaeo.2017.09.006>.
- Patz, J.A., Campbell-Lendrum, D., Holloway, T., Foley, J.A., 2005. Impact of regional climate change on human health. *Nature* 438, 310–317. <https://doi.org/10.1038/nature04188>.
- Paull, C.K., Martens, C.S., Chanton, J.P., Neumann, A.C., Coston, J., Jull, A.J.T., Toolin, L.J., 1989. Old carbon in living organisms and young CaCO₃ cements from abyssal brine seeps. *Nature* 342, 166–168. <https://doi.org/10.1038/342166a0>.
- Peeters, F.J.C., Brummer, G.J.A., Ganssen, G., 2002. The effect of upwelling on the distribution and stable isotope composition of *Globigerina bulloides* and *Globigerinoides ruber* (planktic foraminifera) in modern surface waters of the NW Arabian Sea. *Global Planet. Change* 34, 269–291. [https://doi.org/10.1016/S0921-8181\(02\)00120-0](https://doi.org/10.1016/S0921-8181(02)00120-0).
- Pinto, F., González, A.M., Hernández, M., Larruga, J.M., Cabrera, V., 1996. Genetic relationship between the Canary Islanders and their African and Spanish ancestors inferred from mitochondrial DNA sequences. *Ann. Hum. Genet.* 60, 321–330.
- Poulain, C., Lorrain, A., Mas, R., Gillikin, D.P., Dehairs, F., Robert, R., Paulet, Y.M., 2010. Experimental shift of diet and DIC stable carbon isotopes: influence on shell $\delta^{13}\text{C}$ values in the Manila clam *Ruditapes philippinarum*. *Chem. Geol.* 272, 75–82. <https://doi.org/10.1016/j.chemgeo.2010.02.006>.
- Prendergast, A.L., Azzopardi, M., O'Connell, T.C., Hunt, C., Barker, G., Stevens, R.E., 2013. Oxygen isotopes from *Phorcus* (*Osilinus*) *turbinatus* shells as a proxy for sea surface temperature in the central Mediterranean: a case study from Malta. *Chem. Geol.* 345, 77–86. <https://doi.org/10.1016/j.chemgeo.2013.02.026>.
- Quay, P., Wu, J., 2015. Impact of end-member mixing on depth distributions of $\delta^{13}\text{C}$, cadmium and nutrients in the N. Atlantic Ocean. *Deep. Res. Part II Top. Stud. Oceanogr.* 116, 107–116. <https://doi.org/10.1016/j.dsr2.2014.11.009>.
- R Core Team, 2017. R: A Language and Environment for Statistical Computing.
- Rando, J.C., Cabrera, V.M., Larruga, J.M., Hernández, M., González, A.M., Pinto, F., Bandelt, H.J., 1999. Phylogeographic patterns of mtDNA reflecting the colonization of the Ann. Hum. Genet. 63, 413–428.
- Rein, B., Lückge, A., Sirocco, F., 2004. A major Holocene ENSO anomaly during the Medieval period. *Geophys. Res. Lett.* 31, 2–5. <https://doi.org/10.1029/2004GL020161>.
- Roy, C., Reason, C., 2001. ENSO related modulation of coastal upwelling in the eastern Atlantic. *Prog. Oceanogr.* 49, 245–255. [https://doi.org/10.1016/S0079-6611\(01\)00025-8](https://doi.org/10.1016/S0079-6611(01)00025-8).
- Schlitzer, R., 2018. eGEOTRACES - Electronic Atlas of GEOTRACES Sections and Animated 3D Scenes ([WWW Document]).
- Sharp, Z.D., 2017. Principles of stable isotope geochemistry 1–385. <https://doi.org/10.5072/FK2GB2459F>.
- Sperling, F.N., Washington, R., Whittaker, R.J., 2004. Future climate change of the subtropical North Atlantic: implications for the cloud forests of Tenerife. *Climatic Change* 65, 103–123. <https://doi.org/10.1023/B:CLIM.0000037488.33377.bf>.
- Spero, H.J., Lea, D.W., 1993. Does the carbon isotopic composition of planktonic foraminifera prey affect shell $\delta^{13}\text{C}$ values. *Eos Trans* 74, 183.
- Steens, T.N.F., Ganssen, G., Kroon, D., 1992. Oxygen and carbon isotopes in planktonic foraminifera as indicators of upwelling intensity and upwelling-induced high productivity in sediments from the northwestern Arabian Sea. *Geol. Soc. Spec. Publ.* 64, 107–119. <https://doi.org/10.1144/GSL.SP.1992.064.01.07>.
- Stuiver, M., Pearson, G.W., Braziunas, T., 1986. Radiocarbon age calibration of marine samples back to 9000 cal yr BP. *Radiocarbon* 28, 980–1021. <https://doi.org/10.1017/s003822200060264>.
- Stuiver, M., Polach, H.A., 1977. Discussion: reporting of 14C data. *Radiocarbon* 19, 355–363. <https://doi.org/10.1017/S003822200003672>.
- Stuiver, M., Reimer, P.J., Reimer, R.W., 2020. CALIB 7.1 [WWW program] [WWW Document], 2.15.20. <http://calib.org>.
- Surge, D., Barrett, J.H., 2012. Marine climatic seasonality during medieval times (10th to 12th centuries) based on isotopic records in Viking Age shells from Orkney, Scotland. *Palaeogeogr. Palaeoclimatol. Palaeoecol.* 350–352, 236–246. <https://doi.org/10.1016/j.palaeo.2012.07.003>.
- Swart, P.K., 1983. Carbon and oxygen isotope fractionation in scleractinian corals: a review. *Earth Sci. Rev.* 19, 51–80.
- Swart, P.K., Greer, L., Rosenheim, B.E., Moses, C.S., Waite, A.J., Winter, A., Dodge, R.E., Helmle, K., 2010. The 13C Suess effect in scleractinian corals mirror changes in the anthropogenic CO₂ inventory of the surface oceans. *Geophys. Res. Lett.* 37, 1–5. <https://doi.org/10.1029/2009GL01397>.
- Sydeaman, W.J., García-Reyes, M., Schoeman, D.S., Rykaczewski, R.R., Thompson, S.A., Black, B.A., Bograd, S.J., 2014. Climate change and wind intensification in coastal upwelling ecosystems. *Science* 345, 77–80. <https://doi.org/10.1126/science.1251635>.
- Tao, K., Robbins, J.A., Grossman, E.L., O'Dea, A., 2013. Quantifying upwelling and freshening in nearshore Tropical American environments using stable isotopes in modern gastropods. *Bull. Mar. Sci.* 89, 815–835. <https://doi.org/10.5343/bms.2012.1065>.
- Thornalley, D.J.R., Elderfield, H., McCave, I.N., 2009. Holocene oscillations in temperature and salinity of the surface subpolar North Atlantic. *Nature* 457, 711–714. <https://doi.org/10.1038/nature07717>.
- Trouet, V., Esper, J., Graham, N.E., Baker, A., Scourse, J.D., Frank, D.C., 2009. Persistent positive north atlantic oscillation mode dominated the medieval climate anomaly. *Science* 324, 78–80. <https://doi.org/10.1126/science.1166349>.
- Trouet, V., Scourse, J.D., Raible, C.C., 2012. North Atlantic storminess and atlantic meridional overturning circulation during the last millennium: reconciling contradictory proxy records of NAO variability. *Glob. Planet. Change* 84–85, 48–55. <https://doi.org/10.1016/j.gloplacha.2011.10.003>.
- Tryon, G.W., 1889. *Manual of Conchology, Structural and Systematic: with Illustrations of the Species.* Academy of natural sciences (conchological section).
- Villanueva Guimerans, P., Ruiz Cañavate, A., 1994. Oceanographic characteristics of the canary islands. *Int. Hydrogr. Rev.* LXXI (1), 67–78.
- Wanamaker, A.D., Butler, P.G., Scourse, J.D., Heinemeier, J., Eiríksson, J., Knudsen, K.L., Richardson, C.A., 2012. Surface changes in the North Atlantic meridional overturning circulation during the last millennium. *Nat. Commun.* 3. <https://doi.org/10.1038/ncomms1901>.
- Wefer, G., Berger, W.H., 1991. Isotope paleontology: growth and composition of extant calcareous species. *Mar. Geol.* 100, 207–248.
- Wilke, I., Meggers, H., Bickert, T., 2009. Depth habitats and seasonal distributions of recent planktic foraminifers in the Canary Islands region (29°N) based on oxygen isotopes. *Deep-Sea Res. Part I Oceanogr. Res. Pap.* 56, 89–106.
- WoRMS Editorial Board, 2018. World register of marine species (WoRMS) [WWW document]. <https://doi.org/10.14284/170>.
- Yanes, Y., Yapp, C.J., Ibáñez, M., Alonso, M.R., De-la-Nuez, J., Quesada, M.L., Castillo, C., Delgado, A., 2011. Pleistocene-Holocene environmental change in the Canary Archipelago as inferred from the stable isotope composition of land snail shells. *Quat. Res.* 75, 658–669. <https://doi.org/10.1016/j.yqres.2010.11.004>.